

AD-A164 498

THREE-DIMENSIONAL WAVE PROPAGATION USING BOUNDARY
INTEGRAL EQUATION TECHN. (U) SIERRA GEOPHYSICS INC
REDMOND WA R J APSEL ET AL. SEP 85 SGI-R-85-120

1/1

UNCLASSIFIED

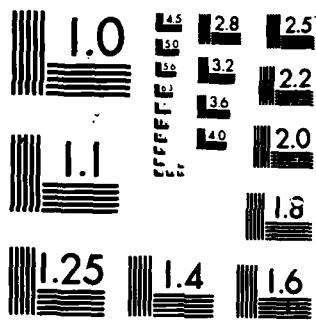
AFGL-TR-85-0245 N00014-84-C-0104

F/G 20/1

NL

END

FORMED
FOR
DPL



MICROCOPY RESOLUTION TEST CHART
NATIONAL BUREAU OF STANDARDS-1963-A

12

AFGL-TR-85-0245

THREE-DIMENSIONAL WAVE PROPAGATION USING
BOUNDARY INTEGRAL EQUATION TECHNIQUES

AD-A164 498

Randy J. Apsel
George R. Mellman
Ping C. Wong

Sierra Geophysics, Inc.
15446 Bel-Red Road
Redmond, Washington 98052

DTIC
ELECTE
FEB 21 1986
S D

September 1985

Scientific Report No. 1

Approved for Public Release; Distribution Unlimited

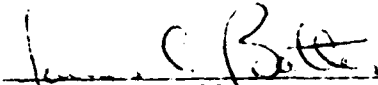
DTIC FILE COPY

AIR FORCE GEOPHYSICS LABORATORY
AIR FORCE SYSTEMS COMMAND
UNITED STATES AIR FORCE
HANSCOM AIR FORCE BASE, MASSACHUSETTS 01731

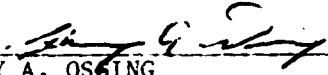
86 2 21 029

CONTRACTOR REPORTS

This technical report has been reviewed and is approved for publication.



JAMES C. BATTIS
Contract Manager



HENRY A. OSING
Branch Chief
Solid Earth Geophysics Branch

FOR THE COMMANDER



DONALD H. ECKHARDT
Director
Earth Sciences Division

This report has been reviewed by the ESD Public Affairs Office (PA) and is releasable to the National Technical Information Service (NTIS).

Qualified requesters may obtain additional copies from the Defense Technical Information Center. All others should apply to the National Technical Information Service.

If your address has changed, or if you wish to be removed from the mailing list, or if the addressee is no longer employed by your organization, please notify AFGL/DAA, Hanscom AFB, MA 01731. This will assist us in maintaining a current mailing list.

REPORT DOCUMENTATION PAGE

1a. REPORT SECURITY CLASSIFICATION Unclassified		1b. RESTRICTIVE MARKINGS	
2a. SECURITY CLASSIFICATION AUTHORITY		3. DISTRIBUTION/AVAILABILITY OF REPORT Approved for public release; distribution unlimited	
2b. DECLASSIFICATION/DOWNGRADING SCHEDULE		5. MONITORING ORGANIZATION REPORT NUMBER(S) AFGL-TR-85-0245	
4. PERFORMING ORGANIZATION REPORT NUMBER(S) Sierra Geophysics Report SGI-R-85-120		7a. NAME OF MONITORING ORGANIZATION Air Force Geophysics Laboratory	
6a. NAME OF PERFORMING ORGANIZATION Sierra Geophysics, Inc.	6b. OFFICE SYMBOL (If applicable) 4R088	7b. ADDRESS (City, State and ZIP Code) Hanscom Air Force Base Massachusetts 01731	
6c. ADDRESS (City, State and ZIP Code) 15446 Bel-Red Road, Suite 400 Redmond, WA 98052		9. PROCUREMENT INSTRUMENT IDENTIFICATION NUMBER F19628-84-C-0104	
8a. NAME OF FUNDING/SPONSORING ORGANIZATION Electronic Systems Div/PKR	8b. OFFICE SYMBOL (If applicable) FQ7620	10. SOURCE OF FUNDING NOS.	
8c. ADDRESS (City, State and ZIP Code) Air Force Systems Command, USAF Hanscom AFB, MA 01731		PROGRAM ELEMENT NO. 61102F	PROJECT NO. 2309
11. TITLE (Include Security Classification) Three-Dimensional Wave Propagation Using Boundary Integral Equation Techniques		TASK NO. G2	WORK UNIT NO. AQ
12. PERSONAL AUTHOR(S) Randy J. Apsel, George R. Mellman, Ping C. Wong			
13a. TYPE OF REPORT Scientific Report #1	13b. TIME COVERED FROM May '84 to May '85	14. DATE OF REPORT (Yr., Mo., Day) 1985 September	15. PAGE COUNT 54
16. SUPPLEMENTARY NOTATION			
17. COSATI CODES		18. SUBJECT TERMS (Continue on reverse if necessary and identify by block number)	
FIELD	GROUP	SUB. GR.	
		Boundary Integral Equation, forward modeling, wave propagation, irregularly layered media	
19. ABSTRACT (Continue on reverse if necessary and identify by block number)			
<p>The efficient numerical propagation of waves in complex three-dimensionally varying environments has been a problem of considerable geophysical interest over the past few years, yet has proven extremely difficult even for the case of acoustic wave propagation in two dimensional structures. This is primarily due to the fact that although the differential equations of motion are linear in the field quantities of interest, they are non-linear in terms of the boundary conditions for most realistic structures. This fundamental nonlinearity precludes construction of the solution for complex structures by superposition of the solutions for simple structures, and forces one into computationally costly schemes.</p> <p>Techniques for dealing with this fundamental nonlinearity have spanned the range from the crudest classical ray tracing approach to the computational-bound finite difference type methods. However, no single technique has ever proven entirely satisfactory for reasons of accuracy, completeness of solution, generality of application, cost or</p>			
20. DISTRIBUTION/AVAILABILITY OF ABSTRACT UNCLASSIFIED/UNLIMITED <input type="checkbox"/> SAME AS RPT <input checked="" type="checkbox"/> OTIC USERS <input type="checkbox"/>		21. ABSTRACT SECURITY CLASSIFICATION Unclassified	
22a. NAME OF RESPONSIBLE INDIVIDUAL Mr. James Battis		22b. TELEPHONE NUMBER (Include Area Code) (617) 861-3767	22c. OFFICE SYMBOL AFGL/LWH

combinations thereof. For example, in cases where significant diffraction and interference effects require "exact" solutions, finite difference techniques have received widespread use. Yet, the finite difference approach is well known for its cumbersome computational demands in two dimensions and almost insurmountable computational demands in three dimensions even on the fastest computers available today.

The heavy computation requirements of the finite difference type methods are created by the necessity of refining the numerical grid proportionately to the wavelengths of interest in all spatial directions, including regions of constant material properties. For problems involving wave propagation in irregular layers of constant material properties within each layer, however, the Boundary Integral Equation (BIE) approach provides a more concise and efficient formulation.

TABLE OF CONTENTS

	<u>Page</u>
1.0 INTRODUCTION	1
1.1 Review of Literature	
1.2 Work Completed to Date	
1.3 Work Currently in Progress	
1.4 Work Planned for Next 12 Months	
2.0 METHODOLOGY	10
2.1 Original Algorithm	
2.2 Improved Algorithm	
2.3 Comparison to Finite Difference	
3.0 RESULTS	29
3.1 Validation Calculations	
3.2 Calculations for AFGL Models	
4.0 REFERENCES	49

Accession For	
NTIS CRA&I	<input checked="" type="checkbox"/>
DTIC TAB	<input type="checkbox"/>
Unannounced	<input type="checkbox"/>
Justification	
By	
Distribution/	
Availability Codes	
Dist	Avail and/or Special
A-1	

1.0 INTRODUCTION

1.1 Review of Literature

The efficient numerical propagation of waves in complex three-dimensionally varying environments has been a problem of considerable geophysical interest over the past few years, yet has proven extremely difficult even for the case of acoustic wave propagation in two dimensional structures. This is primarily due to the fact that although the differential equations of motion are linear in the field quantities of interest, they are non-linear in terms of the boundary conditions for most realistic structures. This fundamental nonlinearity precludes construction of the solution for complex structures by superposition of the solutions for simple structures, and forces one into computationally costly schemes.

Techniques for dealing with this fundamental nonlinearity have spanned the range from the crudest classical ray tracing approach to the computational-bound finite difference type methods. However, no single technique has ever proven entirely satisfactory for reasons of accuracy, completeness of solution, generality of application, cost or combinations thereof. For example, in cases where significant diffraction and interference effects require "exact" solutions, finite difference techniques have received widespread use. Yet, the finite difference approach is well known for its cumbersome computational demands in two dimensions and almost insurmountable computational demands in three dimensions even on the fastest computers available today.

The heavy computation requirements of the finite difference type methods are created by the necessity of refining the numerical grid proportionately to the wavelengths of interest in all spatial directions, including regions of constant material properties. For problems involving wave propagation in irregular layers of constant material properties within each layer, however, the Boundary Integral Equation (BIE) approach provides a more concise and efficient formulation.

Basically, the BIE formulation takes advantage of the fact that the propagation of waves through a region of constant material properties can be treated analytically, leaving only the interactions at the bounding surfaces to be treated numerically. Rather than imposing a grid over the entire volume, the BIE method only requires gridding of the interfaces between regions of constant material properties. Not only are there potential savings in computational effort to solve a smaller system of equations, but the formulation represents a concise treatment of the pertinent physics involved. By virtue of this contraction of information, the smaller matrices in the BIE approach are much denser than the corresponding matrices in the finite difference approach. These dense matrices are typically poorly conditioned and must be given careful consideration during implementation of matrix solution techniques to avoid numerical instabilities.

Various techniques have appeared in the literature for dealing with the dense matrices in the BIE approach. One technique involves introduction of a Kirchhoff approximation into the BIE formalism (eg., Berryhill, 1979; Scott and Helmberger, 1982; Mellman, et al., 1982). In the Kirchhoff approximation the interaction between neighboring points on a boundary is ignored by locally approximating the boundary at each sample point by the tangent plane at that point and then using plane wave reflection and transmission coefficients to compute the unknown boundary values. Even with the Kirchhoff approximation, one is still confronted with the denseness of the matrices used to propagate the boundary values forward to the desired positions. Furthermore, and of utmost importance, is the fact that this decoupling of neighboring boundary points in the Kirchhoff approximation precludes simulation of head waves, surface waves, most diffraction effects and any other dynamic effects related to multiple interactions of the wavefield with a single interface.

A time domain treatment of the full system of equations has been addressed by Cole (1980) for two-dimensional acoustical problems in geophysics. Cole's approach becomes expensive at high frequencies or for late arriving signals as the product of the frequency step times the

time step must be less than about 10 to maintain stability. More importantly, the formulation does not handle the dense matrices efficiently, precluding generalization to three-dimensional elastic multilayered problems. Also, it is difficult to include realistic material attenuation and to suppress late arriving spurious reflections off the artificial extremities of the grid using a time domain formulation.

Ferguson (1982) studied two-dimensional elastic problems using a frequency-domain BIE treatment in which the unknown boundary values are expanded in a series of plane waves with unknown amplitudes determined by performing enormous matrix inversions at each frequency/wavenumber pair to satisfy the boundary conditions. Although realistic attenuation is included, the computational cost of Ferguson's approach is at least an order of magnitude larger than finite difference type methods and provides incorrect results for problems involving interfaces with slopes exceeding about 60 degrees.

Schuster (1984) has formulated a frequency domain BIE approach based on first solving a set of smaller uncoupled singular boundary integral equations for the individual primary responses of each interface and then coupling them together by successive iterations using a Neumann series perturbation treatment. Schuster's method is stable, accurate, nicely convergent and increases in cost linearly with the number of layers, yet the algorithm still requires large matrix inversions for the individual self-interaction operators preventing a cost-competitive alternative to finite difference methods.

Apsel, et al., (1983) formulated a frequency domain BIE approach in which there are no matrix inversions, realistic attenuation is included, the method is stable and accurate and the algorithm is significantly more cost-effective than finite difference type algorithms. A fundamental ingredient in the formulation is the realization that the integrable singularities in the self-interaction operators along each interface have the same convolutional form as those for a flat reference plane. Then instead of perturbing the entire primary response of the individual interfaces as in Schuster's approach (1984), the exact solu-

tion including all kinematic and dynamic effects is obtained iteratively from the singular self-interaction responses using a specially designed perturbation treatment guaranteed to be uniformly and optimally convergent. All matrix inverse operations are reduced to simple deconvolutional operations, which are efficiently handled using Fast Fourier Transform algorithms.

1.2 WORK COMPLETED TO DATE

The BIE formulation presented in Section 4.1 of Apse et al. (1983) has been implemented for 2-D multilayered acoustic geologic structures. There were two significant problems with the original implementation.

First, the Neumann series iterative procedure exhibited poor and often non-existent convergence for models departing even moderately from the flat reference planes. The second problem was the presence of spurious edge reflections for models with interfaces that failed to return to the depths of the reference planes near the horizontal model extremes.

To address the convergence problems, it was necessary to make four improvements to the simple Neumann series iterative procedure. The first improvement was to express the boundary values at the n-th iteration, X_n , as a series of basis vectors, ϕ_i , with unknown coefficients, α_i ,

$$X_n = \sum_{i=1}^n \alpha_i \phi_i \quad (1)$$

in which $\phi_i = ([C][A])^{-1} [C]\{F\}$. The unknown coefficients at the n-th iteration ($\alpha_1, \alpha_2, \dots, \alpha_n$) are determined by minimizing the residual in the boundary integral equations in a least-squared error norm. If all the coefficients were determined to be unity, then the expansion in Eq. (1) would correspond to the Neumann series solution. With variable coefficients at each iteration, the method is guaranteed to be uniformly convergent in the absence of numerical roundoff.

The second improvement was to orthogonalize and normalize the basis vectors in Eq. (1) in order to more rapidly span the solution space. This resulted in approximately a 20 percent improvement in the overall convergence rate.

The third improvement was to implement an automatic restart on the iteration loop to: eliminate the potential roundoff problems; reduce the cost of the least-squares operation at each iteration by limiting the number of iterations to ten per pass; and increase the rate of convergence by iterating on differences of boundary values from previous passes rather than directly on the boundary values. This resulted in approximately a 10 percent improvement in the overall convergence rate.

The fourth improvement was to use the boundary values from previous frequencies to achieve a better starting solution than $[C]^{-1}\{F\}$ at the current frequency. This resulted in approximately a 20 percent reduction in the number of iterations. A further improvement would be possible using more sophisticated extrapolation and phase unwrapping techniques to more closely predict the boundary values at the current frequencies from the boundary values from previous frequencies.

Even though these four improvements provided a much more reliable algorithm, the convergence was still far too slow for models with moderate or large perturbations in interface depths from the flat reference planes.

The second problem area related to spurious edge effects was addressed by padding the models by at least ten percent at both horizontal extremes and applying tapers in the spatial domain to suppress edge reflections. Wrap-around events in the spatial domain caused by the discrete inverse Fourier transforms in the wavenumber deconvolution step at each iteration were completely suppressed by simple padding in the wavenumber domain. Also, potential ringing from the finite Fourier transforms was suppressed by applying tapers at large wavenumbers for the inverse transforms and in the spatial taper zones for the forward transforms.

This combination of tapering and padding was very effective at eliminating spurious edge effects except for models with non-zero relief from the reference planes near the edges of the interfaces. These

remaining spurious effects and the inadequate rate of convergence are being addressed in the work currently in progress as discussed in Section 1.3. The original approach with the flat reference planes is described in more detail in Section 2.1 and the current work is described in more detail in Section 2.2.

Throughout the project, rigorous internal and external validations of the algorithm have been performed. The results from some of the most important validations using the original approach are presented in Section 3.1. Also, some preliminary results on simple models for AFGL are presented in Section 3.2.

1.3 WORK CURRENTLY IN PROGRESS

The outstanding problems discussed in Section 1.2 on the inadequate rate of convergence and the spurious edge effects for models with interfaces that did not coincide with the reference planes are currently being addressed. Both problems were directly related to trying to handle general models with large perturbations in interface depths with respect to the reference planes using basically a perturbation approach. Using the flat layer deconvolutional coefficients to precondition the system of equations did not improve the rate of convergence for models with large perturbations and did not solve the edge effects problem for those models with edge perturbations from the flat reference planes.

To address both problems, the new formulation has eliminated the dependence on the reference planes to suppress edge reflections and an improved iterative solution technique is being implemented to replace the old technique. In the new method, the models are padded at the horizontal extremes with a thin absorption zone at least twenty samples wide in which the forcing functions and integration quadrature coefficients are exponentially tapered to zero at the edges to suppress the spurious edge reflections. The tapers are applied in the frequency domain by prescribing Q values that are tapered to nearly zero in the absorption zone. This is similar to the work of Cerjan, et al. (1985) except that the exponential tapers operate only on the amplitudes and do not affect the phase information.

The improved iterative solution technique is an asymmetric conjugate direction method with an iteration restart capability similar to the original method and a more sophisticated extrapolation of the boundary values from previous frequencies to achieve a closer starting guess at the next frequency. The method is proving to be stable even for the most complex models with convergence rates on the order of the square root of the number of samples per interface. The largest improvement is the more uniform convergence rate provided by more optionally picking new search directions, whereas the rate of convergence would slow down considerably when approaching the true solution in the previous method.

1.4 WORK PLANNED FOR THE NEXT 12 MONTHS

The first task is to fully test the new iterative solution technique and new edge reflection suppression technique in the 2-D acoustic code as described in Section 1.3. This will involve repeating the internal and external validation exercises using the upgraded algorithm. Once successful, various 2-D acoustic simulations of interest to AFGL will be performed.

The next phase of the project would then be to extend the algorithm to the 3-D acoustic case and perform more validation exercises and simulations for 3-D cases. After the 3-D acoustic algorithm is complete, development will begin on the 3-D elastic algorithm.

2.0 METHODOLOGY

2.1 ORIGINAL BINTEQ FORMULATION

The boundary integral equations describing complete wave propagation through arbitrary three-dimensional elastic multilayered media are derived in two steps. First, the known characterization of wave propagation within a single irregular layer is written in terms of integral representations involving the full space Green's functions with properties of that layer. Second, the interaction of the wavefield is simultaneously imposed at all boundaries to satisfy all boundary and continuity conditions leading to a system of Fredholm integral equations of the second kind for the unknown boundary values. Once this system of equations is solved for the unknown boundary values, the wavefield may be propagated from the boundaries to all receiver positions of interest within a given layer using the integral representations of the first step. The formulation for the 2-D and 3-D acoustic cases is analogous to the 3-D elastic case and will not be repeated here.

The model geometry for the wave propagation problem solved in the BIE formulation is depicted in Figure 1 by N irregular layers overlying a semi-infinite half-space. The layers are allowed to pinchout but not to cross in this formulation. Each layer is characterized by constant shear and compressional wave velocities and constant densities. Realistic material attenuation is introduced by allowing the velocities to be complex. Wave propagation within a given layer is expressed in terms of the Green's functions for a full-space with the properties of that layer. The formulation is not restricted to constant material properties within a given layer, although the Green's functions for that case are quite simple. The formulation is carried out for the full elastic case and the corresponding acoustic formulation is obtainable from the derived equations by replacing the vector equations with scalar equations.

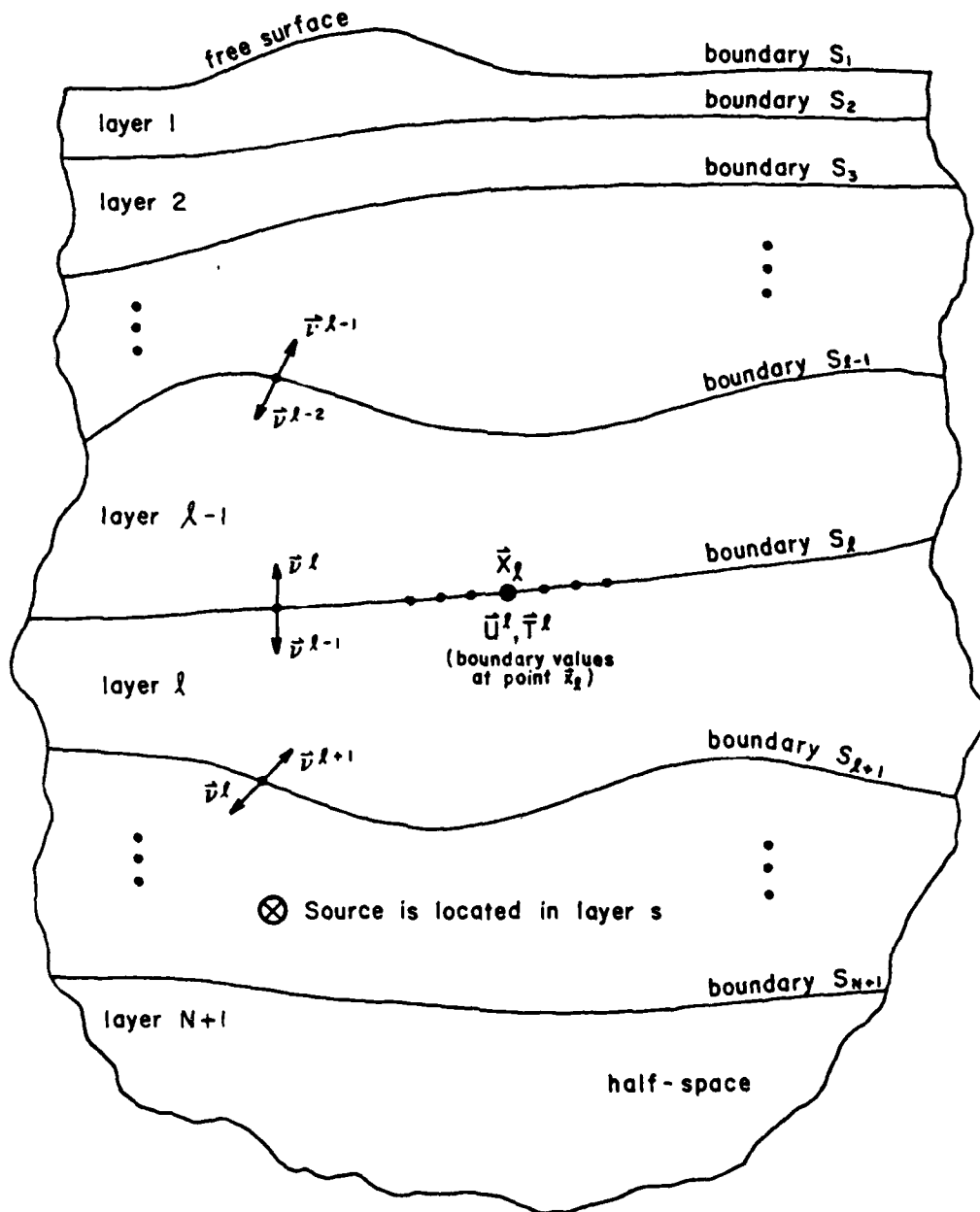


Figure 1. Cross-sectional model geometry for layered half-space used in BIE method formed by N irregular layers overlying a uniform half-space, with each layer characterized by constant material properties. The source and receiver can be located anywhere in the medium.

The first step in the formulation is to write expressions for the displacement field within a single layer without consideration of the boundary interaction. In layer ℓ ($\ell=1,2,\dots,N+1$), the displacement vector must satisfy the homogeneous ($\ell \neq s$) or inhomogeneous ($\ell=s$) equations of motion (depending on whether or not the source layer s is the same as layer ℓ) for a full-space with properties of layer ℓ . The Representation Theorem of Elastodynamics (see, for example, deHoop, 1958) provides an expression for the displacement vector located anywhere within volume V_ℓ containing layer ℓ in terms of integrals of the displacement and traction field over the bounding surface of volume V_ℓ times the corresponding Green's functions for a full-space with properties of that layer. The i -component of displacement at location \vec{x}_ℓ can then be written in the frequency domain using the Representation Theorem for a volume V_ℓ bounded by layer interfaces S_ℓ and $S_{\ell+1}$.

$$\begin{aligned} \varepsilon^\ell(\vec{x}_\ell) U_i^\ell(\vec{x}_\ell) &= \int_{S_\ell} \left[G_{ji}^\ell(\vec{x}_\ell, \vec{y}_\ell) T_j^\ell(\vec{y}_\ell) - H_{ji}^\ell(\vec{x}_\ell, \vec{y}_\ell) U_j^\ell(\vec{y}_\ell) \right] dS(\vec{y}_\ell) \\ &- \int_{S_{\ell+1}} \left[G_{ji}^\ell(\vec{x}_\ell, \vec{y}_{\ell+1}) T_j^{\ell+1}(\vec{y}_{\ell+1}) - H_{ji}^\ell(\vec{x}_\ell, \vec{y}_{\ell+1}) U_j^{\ell+1}(\vec{y}_{\ell+1}) \right] dS(\vec{y}_{\ell+1}) \\ &+ \delta_{\ell s} \int_{V_\ell} \left[G_{ji}^\ell(\vec{x}_\ell, \vec{z}_\ell) f_j(\vec{z}_\ell) \right] dV(\vec{z}_\ell) \end{aligned} \quad (2)$$

($i, j=1,2,3$)

in which the summation over repeated indices is understood, the frequency arguments have been omitted for brevity and

\vec{y}_m = an integration point on bounding surface S_m ;

$G_{ji}^\ell(\vec{x}_\ell, \vec{y}_m)$ = the j -component of the full-space Green's function displacement vector at location \vec{y}_m on surface S_m due to point force in the i -direction at location \vec{x}_ℓ with properties of layer ℓ ;

$H_{ji}^{\ell}(\vec{x}_{\ell}, \vec{y}_m)$ = the j-component of the corresponding Green's function traction vector formed from the inner-product of the kj-component of the Green's function stress tensor G_{kji}^{ℓ} at location \vec{y}_m on surface S_m with the k-component of the unit upward normal \vec{v}_k^m at point \vec{y}_m (summing over $k=1,2,3$);

$U_j^m(\vec{y}_m)$ = the j-component of displacement at location \vec{y}_m on surface S_m ;

$T_j^m(\vec{y}_m)$ = the j-component of the corresponding traction at location \vec{y}_m on surface S_m formed from the inner-product of the kj-component of the stress tensor with the k-component of the unit upward normal \vec{v}_k^m at point \vec{y}_m (summing over $k=1,2,3$);

$f_j(\vec{z}_{\ell})$ = the j-component of the source function at location \vec{z}_{ℓ} anywhere in layer ℓ (assuming the source is a Delta-function in space, then the volume integral reduces to the evaluation of the integrand at point \vec{z}_{ℓ});

δ_{ls} = 0, if $l \neq s$
1, if $l = s$, s = source layer number;

$\epsilon^{\ell}(\vec{x}_{\ell})$ = 1, if \vec{x}_{ℓ} inside layer ℓ
 $\frac{1}{2}$, if \vec{x}_{ℓ} on surface bounding layer ℓ
0, if \vec{x}_{ℓ} outside layer ℓ .

In Eq. (2), the layer comprising volume V_{ℓ} is assumed to extend to infinity at the horizontal extremes to eliminate the surface integrals along those portions of the surface bounding volume V_{ℓ} and the negative sign for the integral over surface $S_{\ell+1}$ is associated with using the upward normal $\vec{v}^{\ell+1} = -\vec{v}^{\ell}$ in the definition of the traction components. Once the boundary values for $U_j^m(\vec{y}_m)$ and $T_j^m(\vec{y}_m)$ are determined for bounding interfaces S_{ℓ} and $S_{\ell+1}$, Eq. (1) can then be used to obtain the displacement field at any point \vec{x}_{ℓ} within layer ℓ . Expressions for the full-space Green's functions with constant material properties are given in Appendix A of Apsel, et al. (1983) for two and three dimensional wave propagation in elastic as well as acoustic media. This completes the propagation step of the BIE formulation and what remains is to impose the boundary interaction coupling.

The boundary interaction coupling requires simultaneous satisfaction of a tractionless free surface (interface 1) and continuous displacements and tractions across each layer interface (2,3,...,N+1). The coupled boundary integral equations arising from the zero traction conditions along the free surface are obtained by evaluating Eq. (1) in volume V_1 (layer 1) at a discrete number (q_1) of observation points \vec{x}_1 along surface S_1 and imposing the zero traction condition, $T_j^1(\vec{y}_1) = 0$, ($j=1,2,3$), for all quadrature points \vec{y}_1 on surface S_1 . This leads to a simultaneous set of $3q_1$ Fredholm integral equations of the second kind for the same number of unknown displacement boundary values U_j^1 , $j=1,2,3$, on surface S_1 , which are coupled to the unknown boundary values on surface S_2 through the integral over surface S_2 .

The coupled boundary integral equations arising from the continuity conditions across each layer interface, S_ℓ ($\ell=2,3,\dots,N+1$), are obtained by evaluating Eq. (2) in volumes $V_{\ell-1}$ and V_ℓ (layers $\ell-1$ and ℓ) at a discrete number (q_ℓ) of observations \vec{x}_ℓ along common surface S_ℓ and imposing the natural boundary conditions of continuous displacements and tractions, $U_j^{\ell-1}(\vec{x}_\ell) = U_j^\ell(\vec{x}_\ell)$ and $T_j^{\ell-1}(\vec{x}_\ell) = T_j^\ell(\vec{x}_\ell)$, $j=1,2,3$, for all quadrature points \vec{y}_ℓ on surface S_ℓ . This leads to a simultaneous set of $6q_\ell$ Fredholm integral equations of the second kind for the same number of unknown displacement and traction boundary values, U_j^ℓ and T_j^ℓ , $j=1,2,3$, on surface S_ℓ , which are coupled to the unknown boundary values on surfaces $S_{\ell-1}$ and $S_{\ell+1}$ through the integrals over surfaces $S_{\ell-1}$ and $S_{\ell+1}$, respectively. Note that when $\ell=2$, the integrals involving $T_j^{\ell-1}(\vec{y}_{\ell-1})$ are identically zero because of the tractionless free surface conditions. Also, note that when $\ell=N+1$, the integrals over surface $S_{\ell+1}$ vanish by virtue of the radiation conditions implicit in the Green's functions for the underlying semi-infinite space.

When the entire discrete set of boundary and continuity conditions is simultaneously imposed, one obtains a coupled system of singular Fredholm integral equations of the second kind for the unknown boundary values along all the interfaces, which can be written in matrix notation as:

$$[I_2]\{U\} = [G]\{T\} - [H]\{U\} + \{F\} \quad (3)$$

in which $[I_2]$ is a di-diagonal matrix consisting of the $\epsilon^{\rho} = 1/2$ factors obtained when specializing Eq. (2) to points on the interfaces; $[G]$ and $[H]$ are the block tri-diagonal displacement and traction Green's function matrices, respectively; $\{F\}$ is the forcing vector consisting of the direct source contributions at nodes only on the interfaces bounding the source; and $\{U\}$ and $\{T\}$ are the unknown displacement and traction boundary value vectors, respectively, at all nodes in the model. The singularities occur in $[G]$ and $[H]$ when quadrature point \vec{y}_m approaches observation point \vec{x}_m in the self-interaction integrals along each interface and in the propagation integrals between adjacent interfaces for the special case of a layer pinchout.

The original BINTEQ solution to Eq. 3 was formulated to meet four objectives:

- 1) optimize computational speed;
- 2) minimize memory requirements for efficient execution in array processors and/or multi-user environments;
- 3) suppress spurious edge effects from the horizontal finiteness of the numerical grid;
- 4) generate accurate complete solutions including all possible kinematic and dynamic effects;

To accommodate these objectives, the BINTEQ formulation proceeded by recognizing that the singular self-interaction elements of matrices $[G]$ and $[H]$ are identical in the limit to those for a flat reference plane with the same upper and lower material properties as the interface being considered. The rows of the self-interaction matrices for layer interfaces are simple convolutional operators and are ideal for preconditioning the original matrix equation. Therefore, by subtracting the self-interaction matrices for flat planes referenced to each interface from both sides of Eq. (3), the system of equations can be rewritten as:

SGI-R-85-120

$$[C]\{\phi\}_{i+1} = [\tilde{A}]\{\phi\}_i + \{F\} \quad (4)$$

in which $[C]$ is a block diagonal matrix containing the $1/2$ factors from $[I_2]$ and the singular convolutional coefficients from the flat self-interaction matrices; $[\tilde{A}]$ is the combined perturbation Green's function matrix obtained by subtracting the flat self-interaction matrices from $[G]$ and $[H]$; and $\{\phi\}$ is the combined vector of unknown displacement and traction boundary values $\{U\}$ and $\{T\}$.

For models with small perturbations from the flat reference planes, the preconditioned system of equations in Eq. (4) is more numerically tractable and is well suited to satisfy all four objectives simultaneously. The interaction singularities are analytically integrable and appear only in the convolutional matrix $[C]$ and the pinchout singularities (if any exist) are also analytically integrable and appear only in perturbation matrix $[\tilde{A}]$. If it could be guaranteed that the norm of the $[\tilde{A}]$ matrix is always less than the norm of the $[C]$ matrix, then Eq. (4) could be solved as accurately as desired using the following iterative Neumann series solution technique with $\{\phi\}_0 = 0$ to initialize the series: first the solution from iteration i , $\{\phi\}_i$, is recursively passed through the right-hand-side of Eq. (4); then the right-hand-side is transformed into the horizontal wavenumber domain using a discrete FFT algorithm; then an updated solution $\{\phi\}_{i+1}$ is immediately obtained by applying the deconvolutional coefficients of the $[C]$ matrix in the wavenumber domain; and then the updated solution is transformed back into the spatial domain for the next iteration.

This procedure would satisfy the first objective by: (a) eliminating all matrix inversion operations; (b) saving the nonzero perturbation submatrices of $[\tilde{A}]$ in the spatial domain and the nonzero deconvolutional coefficients of $[C]$ in the wavenumber domain for recursive iterations and multiple sources; (c) reducing the number of iterations of the precondition system relative to the original system; and (d) using an array processor to rapidly calculate the nonzero elements of $[\tilde{A}]$ and $[C]$, process all the required FFTs and perform all the required complex matrix/vector multiplies.

This procedure also satisfies the second objective by: (a) saving nontrivial perturbation submatrices and deconvolutional coefficients on disk if memory is insufficient; and (b) the largest in-core memory requirement is governed merely by a single complex multiplication of a submatrix times a boundary value subvector.

To understand how the third objective is satisfied, it is instructive to consider the origins of the three possible types of spurious edge effects. First, edge reflections from the deconvolutional operation on the forcing vector $\{F\}$ during the first iteration are possible for forcing vectors without compact support, which would usually be the case except possibly for structures with significant amounts of material attenuation in the source layer (i.e., low Q values). Second, edge reflections are similarly possible when updating the right-hand-side of Eq. (4) if the perturbed Green's function integration operators in $[\tilde{A}]$ do not have compact support. Third, spatial wraparound effects are possible if the convolutional coefficients are not sufficiently padded with zeroes. It should also be pointed out that for interfaces which return to their respective flat reference planes at both horizontal extremes, the second type of edge reflections would require less care than the first type. Therewith, the second objective is correspondingly satisfied by: (a) extending the model somewhat at the horizontal extremes with and tapering the forcing functions and perturbed integration operations to zero; (b) tapering the convolutional coefficients; and (c) padding the convolutional coefficients and the right-hand-sides with zeroes out to twice the model size to totally prevent the circular deconvolution process in the wavenumber domain from wrapping any arrivals back into the model.

As mentioned previously, if one could guarantee that the norm of $[\tilde{A}]$ be less than the norm of $[C]$, then the iterative Neumann series solution technique would converge rapidly and uniformly to the exact solution and the fourth objective would be met automatically. However, this cannot always be guaranteed especially for large model perturbations away from the flat reference planes. In Schuster's iterative BIE solution technique, the Neumann series is guaranteed to

be uniformly convergent because the full interaction submatrices are inverted, leaving only the coupling between interfaces to control the rate of convergence. As will be seen shortly, however, Schuster's approach is extremely inefficient because of having to perform the matrix inversions and furthermore, there are alternatives to the Neumann series expansion which are guaranteed to be uniformly convergent. The alternative adopted for the original BINTEQ formulation is to expand the unknown boundary values in a series of basis vectors with unknown coefficients as shown in Eq. (1) in Section 1.2. Each basis vector is generated recursively as described above for the Neumann method and is made orthogonal to all previous basis vectors using a modified Gram-Schmidt orthogonalization procedure. The unknown basis vector coefficients are determined at a given iteration to satisfy the boundary and continuity conditions implicit in Eq. (4) in a least-squared error norm. To avoid numerical roundoff problems, an automatic restart on the iteration loop is required whenever the condition number of the least-squares system for the unknown coefficients exceeds single precision accuracy. The iterated solution contains all the possible arrivals (e.g., direct waves, multiples, converted phases, head waves, diffractions and surface waves). Once all the boundary values are determined at a given frequency, the field at any location \vec{x}_ℓ within any layer ℓ may be obtained by evaluating Eq. (2). Time domain response would be obtained through discrete Fourier synthesis.

The main problem with this procedure is the requirement that the perturbations of the irregular interfaces from the flat reference planes be small at the center of the model and zero at the edges. Otherwise, the preconditioning from subtracting the flat self-interaction matrices would not improve the rate of convergence and the simple tapering described above would be insufficient to suppress all the spurious edge effects. Because the basis vectors are recursively dependent on the flat layer self-interaction solution ($[C]^{-1}\{F\}$), the more iterations required to satisfy the desired error tolerance, the slower the rate of convergence. Therefore the rate of convergence is model dependent and is too slow for practical applications using this original procedure.

Improvements to the iterative procedure are currently being worked on as described in the following section.

2.2 IMPROVED BINTEQ FORMULATION

The preconditioning of the system of equations in Eq. (4) is physically motivated and useful only for small perturbation problems with respect to the flat reference planes. To solve the more desirable general layered cases more efficiently, it was necessary to choose a more reliable preconditioning technique and an iterative scheme that more rapidly spans the solution space.

First, the flat layer reference planes are being eliminated and a more robust technique is being implemented to suppress the spurious edge reflections. The layers are padded at the horizontal extremes with thin absorption zones in which the Q values for the layer are smoothly tapered to a small waterlevel value at the edge of the model. This introduces an extra exponential decay into the forcing functions and Green's function integration operators which gradually reduces the amplitudes of the boundary values in the absorption zone. The waterlevel value is set at each frequency such that any spurious edge reflections are too small to contaminate the real signal.

The implementation of the absorption zones is portrayed in Figure 2 for observation point \vec{Y}_ℓ in the absorption zone and source point \vec{X}_m in the original unpadded model. Defining A_z to be the width of the absorption zone (typically the greater of 20 samples or 10 percent of the model width in that direction), the Q -values at position $\vec{Y}_{\ell j}$ in the absorption zone are given by

$$Q_{\ell j} = Q_\ell \left\{ (1-W_\ell) \left[\cos \frac{\pi}{2} \cdot \frac{|\vec{Y}_{\ell j} - \vec{Y}_t|}{A_z} \right]^{s_\ell} + W_\ell \right\} \quad (5)$$

in which " W_ℓ " is the waterlevel factor, s_ℓ controls the power of the decay and \vec{Y}_t signifies the horizontal starting position of one of the absorption zones or \vec{X}_m , if \vec{X}_m is within the absorption zone. Therefore, the Q -values are smoothly tapered from a value of Q_ℓ at the start of the absorption zone to WQ_ℓ at the end of the absorption zone.

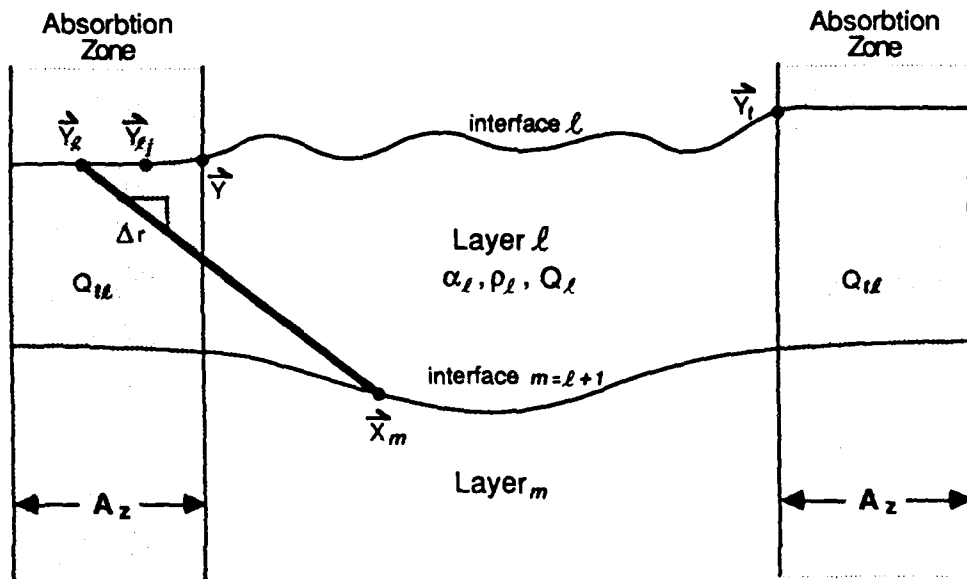


Figure 2
Geometry and notation used for horizontal absorption zones.

The differential amplitude reduction factors, RF, for the Green's functions are then given by multiplying the N reduction factors for the N cells between \vec{Y}_ℓ and \vec{Y}_t :

$$RF(\vec{X}_m, \vec{Y}_\ell) = e \left[-\frac{\omega \Delta r}{2\alpha_\ell} \sum_{j=1}^N \left(\frac{1}{Q_{\ell j}} - \frac{1}{Q_\ell} \right) \right] \quad (6)$$

for which ω is the angular frequency and Δr is the slant distance along each of the cells contributing to the reduction factor. The waterlevel factor, W_ℓ , is computed to make the reduction less than or equal to 0.1 for the last cell's contribution:

$$W_\ell = \left[\frac{-2\alpha_\ell Q_\ell \ln(0.1)}{\omega \Delta X} + 1 \right]^{-1} \quad (7)$$

If ΔX is different from ΔY for 3-D models, then W_ℓ would be calculated separately in the two horizontal directions. The power s_ℓ is computed such that $Q_{\ell j} = 0.1 (1 - W_\ell) Q_\ell$ at the mid-point of the absorption zone in order to provide gradual reduction factors throughout the absorption zone.

This procedure to suppress edge reflections is similar to the work of Cerjan, et al. (1985), with two exceptions. First, the constants in the exponential reduction factors are based on physical quantities in the present approach and do not alter the phase information. Second, there is no need for an absorbing zone at the bottom of the models because the radiation conditions are handled exactly by the Green's functions for the underlying half-space layer. This new procedure is in the process of being tested and some of the constants may need to be altered for optimal suppression of the spurious edge reflections.

Along with the new edge reflection suppression procedure, a new iterative solution technique is being implemented and tested. The largest problems with the original iterative solution technique were: (1) using basically a perturbation method on models with moderate or large perturbations in the interface depths with respect to the flat reference planes; (2) less than optimal preconditioning of the matrix equations for these non-perturbation problems; and (3) no facility to pick optional search directions for the successive iterations. In the new method, a conjugate gradient iterative solution technique is used instead and the singular diagonal terms are used to precondition the system of equations.

Numerically, the problem with the original method was that the search directions became too similar at successive iterations causing prohibitively slow convergence in many cases. This is the same type of problem encountered in using the method of steepest descent where minimization in the gradient direction causes convergence back and forth across the valley rather than more directly down the valley. The conjugate gradient (CG) method provides a framework for picking the search directions to minimize the residuals more rapidly while still guaranteeing uniform convergence.

To derive the CG solution, Eq. (3) is recast into the simple form:

$$A X = B \quad (8)$$

in which A is a general, asymmetric complex matrix containing the Green's function integration submatrices from $[G]$ and $[H]$ and the ε -factors from $[I_2]$, B is the forcing vector $\{F\}$, and X is the unknown boundary value vector. The standard CG method is for symmetric positive definite matrix equations. Before deriving the generalization to the asymmetric case, the basic formulae and properties of the CG solution will be discussed for the normal equations:

$$A^T A X = A^T B \quad (9)$$

in which superscript T indicates the complex-conjugate transpose matrix. A good reference for the symmetric CG solution to Eq. (9) can be found in Chapter 10 of Golub and van Loan (1983). The basic approach is to span the solution X by a set of mutually A-orthogonal search directions P_n , ($n=1,2,\dots$)

$$X_n = X_{n-1} + \alpha_n P_n, \quad X_0 = \text{best estimate}, \quad (10)$$

with the corresponding residual vector $r_n = A^T(B - AX_n)$ given by

$$r_n = r_{n-1} - \alpha_n A^T A P_n, \quad r_0 = A^T(B - AX_0) \quad (11)$$

To directly minimize the residual vector in Eq. (11), the coefficients are found by requiring that $(P_n, r_n) = 0$ to give

$$\alpha_n = \frac{(P_n, r_{n-1})}{(AP_n, AP_n)} = \frac{(r_{n-1}, r_{n-1})}{(AP_n, AP_n)} \quad (12)$$

in which the second form is derived by using Eq. (14) and induction arguments and the notation (X, Y) denotes the inner product $X^T Y$. What remains is how to define the optimum search directions that satisfy the A-orthogonality condition:

$$(AP_i, AP_j) = 0 \text{ for } i \neq j \quad (13)$$

To reduce the residuals as rapidly as possible, it is desirable to choose the search directions P_n to be the closest vectors to r_{n-1} that still satisfy Eq. (13). With no loss in generality, the search directions can be written recursively as:

$$P_n = r_{n-1} + \beta_n P_{n-1}, \quad P_1 = r_0 \quad (14)$$

Applying Eq. (13) with $i = n$, introducing P_n from Eq. (14) and $A^T A P_j$ from Eq. (11), using induction arguments for $j < n$ and the orthogonality of the residual vectors $(r_i, r_j) = 0$ for $i \neq j$ directly gives the coefficients β_n :

$$\beta_n = \frac{(r_{n-1}, r_{n-1})}{(r_{n-2}, r_{n-2})}, \quad (n = 2, 3, \dots). \quad (15)$$

To optimize the rate of convergence, the system of equations in Eq. (11) is preconditioned by the diagonal elements and the initial estimate is derived by extrapolating the amplitude and phase information from the solution at previous frequencies.

Note that this CG algorithm for the normal equations requires two matrix-vector multiplications for each iteration because of the $A^T A P_n$ term. An additional drawback of solving the normal equations is that the rate of convergence is governed by the square of the condition number of the A-matrix instead of just the condition number with an asymmetric algorithm.

The derivation of the asymmetric CG method is similar to the symmetric case in Eqs. (10) through (15) with a few basic changes. As before, the solution is expanded in a set of A-orthogonal search directions P_n , ($n=1, 2, \dots$) with coefficients α_n :

$$X_n = X_{n-1} + \alpha_n P_n, \quad X_0 = \text{best estimate}, \quad (16)$$

with residual vector $r_n = B - A X_n$ given by

$$r_n = r_{n-1} - \alpha_n A P_n, \quad r_0 = B - A X_0. \quad (17)$$

In this case the coefficients α_n are determined to minimize the residual vector in Eq. (17) in a least-squared error sense to give:

$$\alpha_n = \frac{(AP_n, r_{n-1})}{(AP_n, AP_n)} \quad (18)$$

Without symmetry arguments, the search directions, P_n , depend on all previous search directions to satisfy Eq. (13):

$$P_n = r_{n-1} + \sum_{i=1}^{n-1} \beta_{in} P_i, \quad P_1 = r_0 \quad (19)$$

Now, applying Eq. (13) with $i=n$ and $j = 1, 2, \dots, n-1$ gives $n-1$ decoupled equations for the $n-1$ coefficients β_{in} at iteration n :

$$\beta_{in} = \frac{-(Ar_{n-1}, AP_i)}{(AP_i, AP_i)}, \quad i=1, 2, \dots, n-1 \quad (20)$$

This asymmetric procedure has the distinct advantage of only one matrix-vector multiplication per iteration (Ar_{n-1} is obtained from Eq. (19) in terms of the stored AP_i vectors, $i = 1, \dots, n$). Furthermore, the rate of convergence is governed by the condition number of matrix A instead of $A^T A$, which results in a substantial improvement over the normal equations. Again, as in the normal equations, the rate of convergence and number of iterations is significantly improved by preconditioning Eq. (10) by the diagonal elements and making good extrapolations for X_0 from previous frequencies.

The rate of convergence can slow down in the asymmetric algorithm when the angle between r_{n-1} and AP_n is sufficiently small that the incremental reductions in the residue from successive iterations is negligible. If this condition ever occurs before desired convergence is reached, the iteration loop is restarted with the latest approximation as the initial estimate and the initial search direction in Eq. (19) is modified for the restart to maximize (AP_n, r_{n-1}) . One method to

modify the search directions is to replace r_{n-1} in Eqs. (19) and (20) with $A^T r_{n-1}$, which essentially switches the method to the symmetric case for one iteration. Again, this procedure is still in testing and other possibilities may be equally plausible.

2.3 COMPUTATIONAL COMPARISONS

The remainder of this section will discuss why BINTEQ represents the optimal BIE formulation in terms of execution time to generate the exact solution. A theoretically straightforward inversion to solve the linear system in Eq. (2) would have been extremely computational inefficient and numerically ill-conditioned because it would have entailed solving an enormous singular system of $(6N+3)q \times (6N+3)q$ complex equations for the $(6N+3)q$ unknown displacement and traction boundary values, with "N" being the number of layers and "q" being the average number of nodes on one interface. Any full inversion type approach would require on the order of $(6N+3)^3 q^3$ floating point operations per frequency compared to about $144Nq^2 P$ for the BINTEQ solution technique, with P being the number of iterations. For example, with $N=5$ and $q=256$, the full inversion requires about 5×10^{11} operations per frequency whereas the BINTEQ technique would require about 1×10^9 operations with $P=20$ iterations per frequency. Furthermore, the overall cost of a BINTEQ calculation is controlled by the speed of repetitively multiplying $3q \times 3q$ complex matrices times $3q \times 1$ complex vectors and is ideally suited to execute with an array processor. Using an FPS AP-120B array processor, this sample problem would take about 100 seconds per frequency, using BINTEQ, which is significantly faster than a typical elastic finite difference type calculation with full volume gridding. Compared to other BIE techniques and assuming adaptability to achieve the high compute rates of the referenced array processor, Ferguson's full inversion algorithm (1982) is estimated to take about 13 hours per frequency for this problem; Schuster's approach (1984) is estimated to take about 4 hours per frequency for this problem based on $(1728N+432)q^3 + 72Nq^2 P$ floating point operations per frequency because of the N complex $6q \times 6q$ interface interaction matrix inversions and the complex $3q \times 3q$ free surface interaction matrix inversion.

3.0 RESULTS

3.1 VALIDATION CALCULATIONS

Since the improved method is still in the final development and testing stages, the validation exercises from the original BINTEQ method will be described in this section. There are very few exact solutions available for checking the algorithm. Therefore, the philosophy of the validation stage has been to perform as many internal checks as possible while at the same time comparing solutions against those from established and available algorithms.

An exhaustive set of internal checks of the BINTEQ algorithm have been completed for the 2-D acoustic code: verification that the free surface boundary conditions and the continuity conditions are being satisfied for a wide range of problems; verification that the effects of varying impedance contrasts from no contrast to a range of contrasts are correct; verification that the lower limit of two nodal points per wavelength produces the same results as finer sampling for the same structure (although user may occasionally use finer sampling to avoid spatial aliasing with structures having very steeply sloping irregularities); verification that there are no spurious edge reflections contaminating solution for a wide range of conditions including very high material attenuation ($Q = 10$) to almost no material attenuation ($Q = 2000$); verification that extra padding at edge of model has no effect on results; and numerous other verifications.

External validations have included: verification of all arrivals for problems with exactly flat interfaces including head waves and Stoneley waves against Sierra Geophysics' VESPA_{TM} algorithm (Apsel, 1982) which simulates complete solutions in flat multilayered viscoelastic structures; verification of geometrical arrival times and amplitudes for a wide range of problems with irregular interfaces against Sierra Geophysics' QUIK_{TM} three-dimensional raytracing algorithm (Lundquist, et al., 1982); and verification of all arrivals including diffractions against a limited set of available finite difference calculations.

Figure 3 shows the model geometry for the flat layer comparison to the exact VESPA solution. The source is located just beneath the interface at a depth of 350 meters at an offset of 500 meters. Receivers are located across the free surface from offsets of 600 out to 2100 meters. The compressional velocities are 5 km/sec and 10 km/sec for layers 1 and 2; densities are 2.0 gm/cc and 2.5 gm/cc; quality factors (Q) are 100 and 1000; the layer thickness is 300 meters. The simulations include frequencies from 10 to 100 Hz. Figures 4 and 5 show the BINTEQ and VESPA shot records, respectively for all 80 receivers and travel times ranging from 0.0 to 0.8 seconds. The traces have been convolved with a Ricker wavelet with a center frequency of 50 Hz. The BINTEQ solution in Figure 4 has been scaled by a time ramp to amplify the late arrivals and the 3-D VESPA solution in Figure 5 has been scaled by an extra square root of time to approximately account for the differences in 2-D and 3-D geometrical spreading. The first event is the direct compressional arrival that is refracted up to the free surface through the interface. The event moving out at the slower 5 km/sec velocity starting at 0.1 seconds and group 21 is a non-geometrical arrival that "tunnels" through the interface. The fact that BINTEQ is able to model such non-geometrical arrivals is quite encouraging for the method. The next four events beginning at 0.18, 0.30, 0.42 and 0.54 are multiples of order 1 through 4 reverberating in the top layer. The excellent agreement with the exact VESPA solution lends considerable confidence in the method.

Figures 6, 7, and 8 repeat the same validation study except that a 200 meter thick basin has been placed on the interface as shown in Figure 6. This time the BINTEQ solution in Figure 7 is being compared against the QUIK raytracing solution in Figure 8 which provides only geometrical arrivals. All other parameters are the same as for the flat layer comparison. The agreement is excellent for the geometrical arrivals modeled by the QUIK raytracing code. Notice how BINTEQ gets continuous events including all diffracted energy off the corners of the basin whereas the raytracing code is unable to model the diffracted energy. For example, the gap in the QUIK solution at 0.1 seconds and groups 29 through 36 is where the smaller diffracted event through the

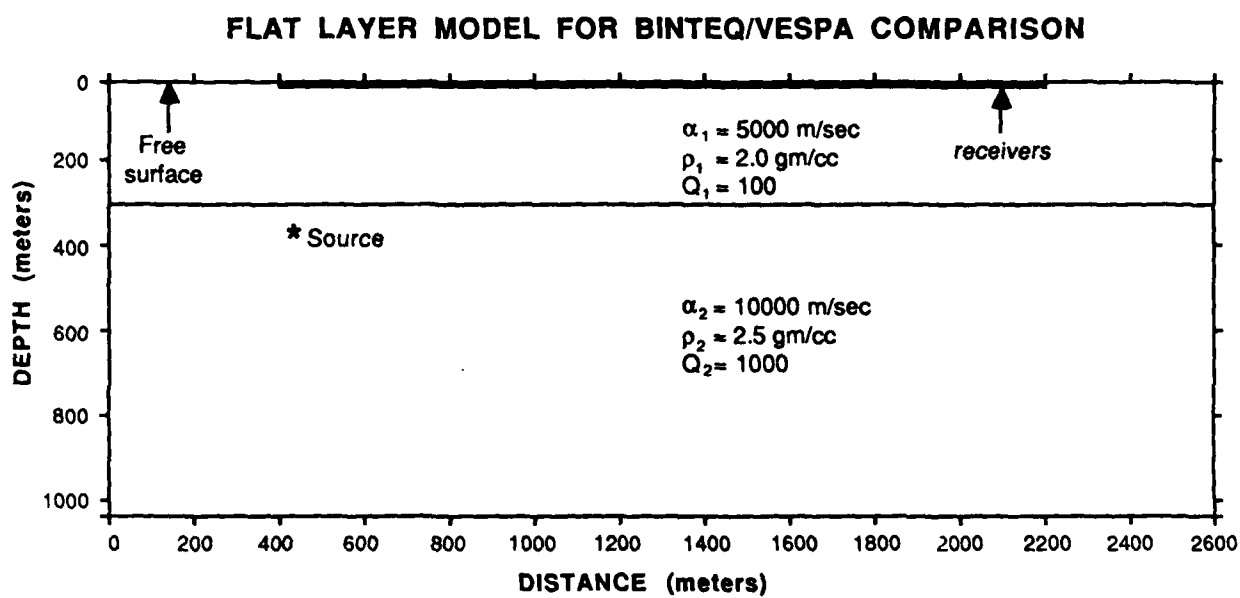


Figure 3

Model geometry for the flat layer validation study between BINTEQ and VESPA shown in Figures 4 and 5.

BINTEQ: SEISMIC SHOT RECORD FOR FLAT LAYER MODEL
COMPLETE SOLUTION FOR NEAR-SURFACE GROUPS
PRESSURE COMPONENT FOR POINT SOURCE AT 350 METER DEPTH

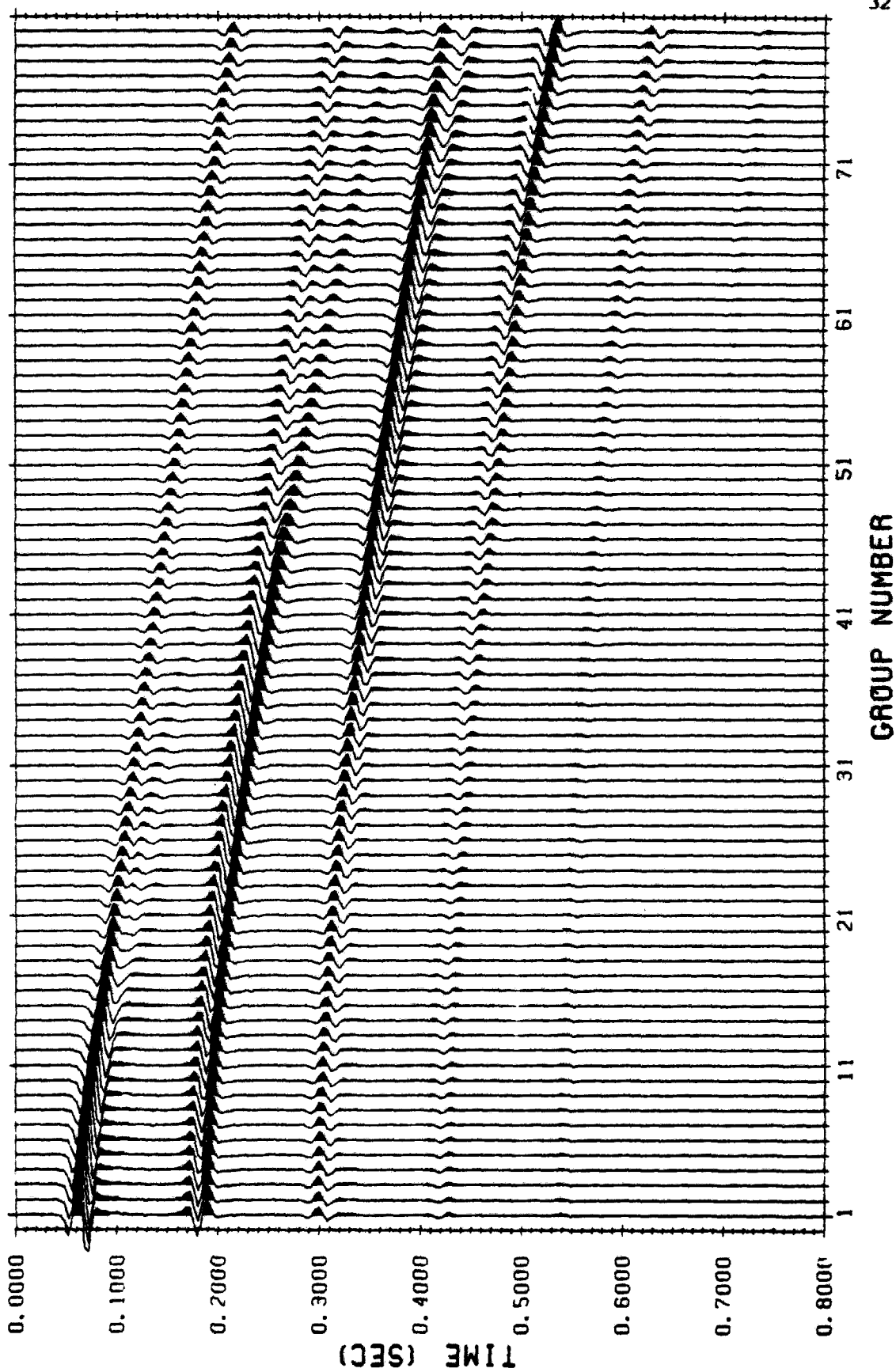


Figure 4
BINTEQ solution for the flat model shown in Figure 3.

VESPA: COMPARISON TO BINTEQ FOR SIMPLE 2-LAYER MODEL
HORIZONTAL SEISMIC SECTION: DEPTH = 20.00
SZZ FOR EXPLOSION DEPTH = 350.0

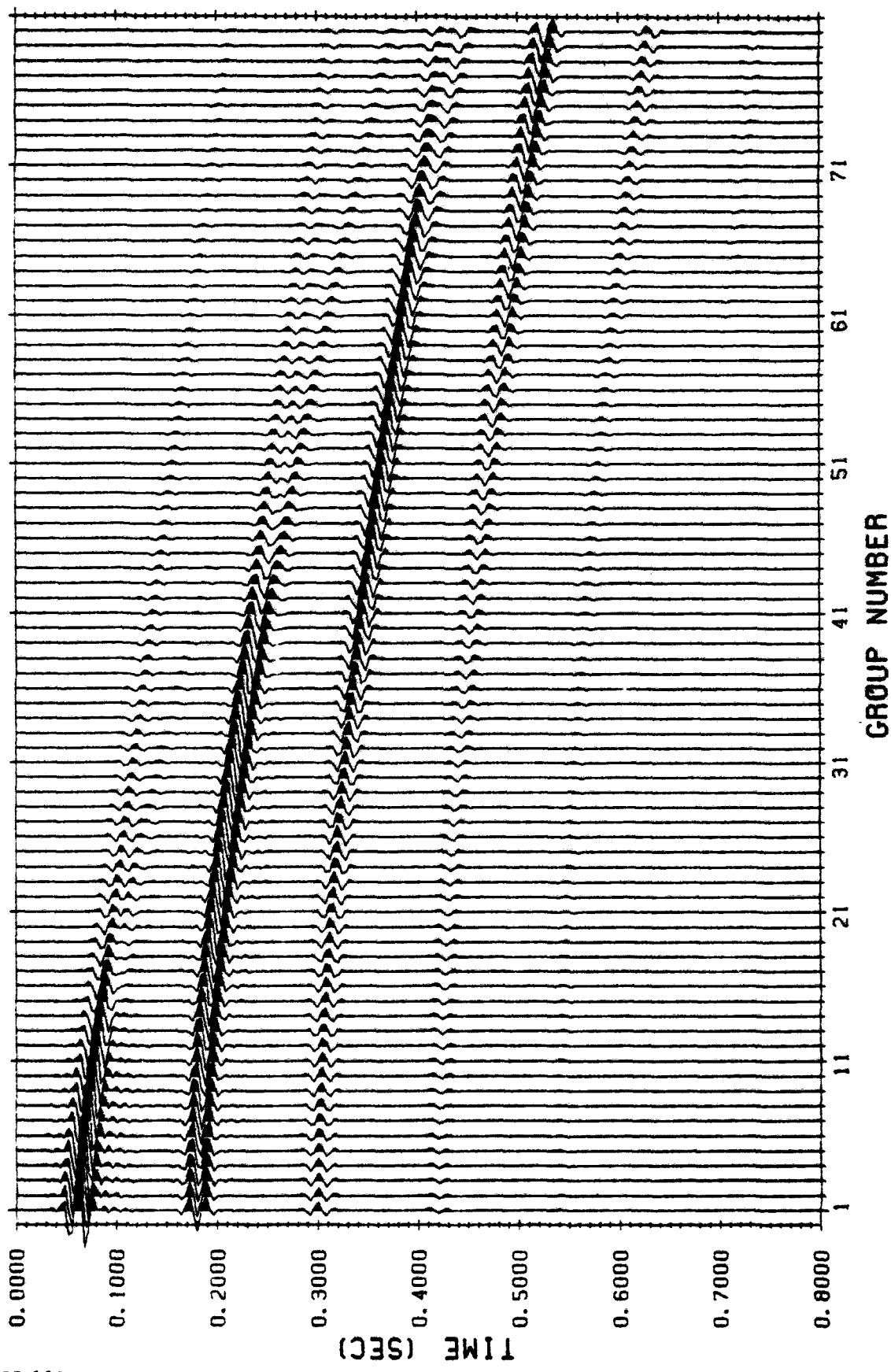


Figure 5
VESPA exact solution for the flat model shown in Figure 3.

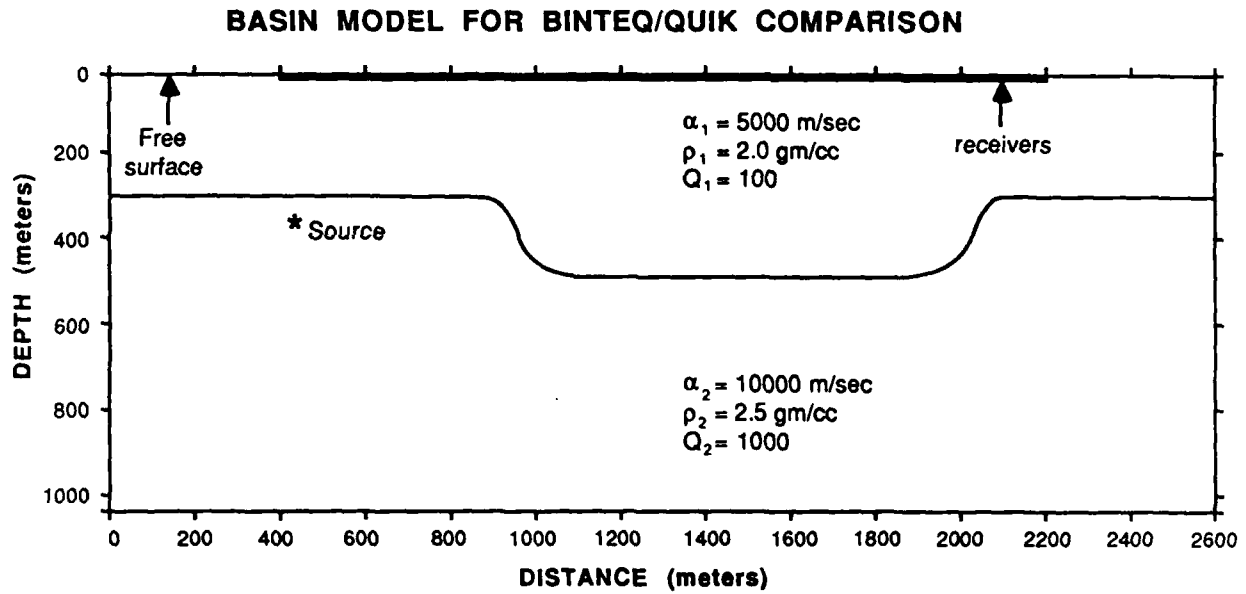
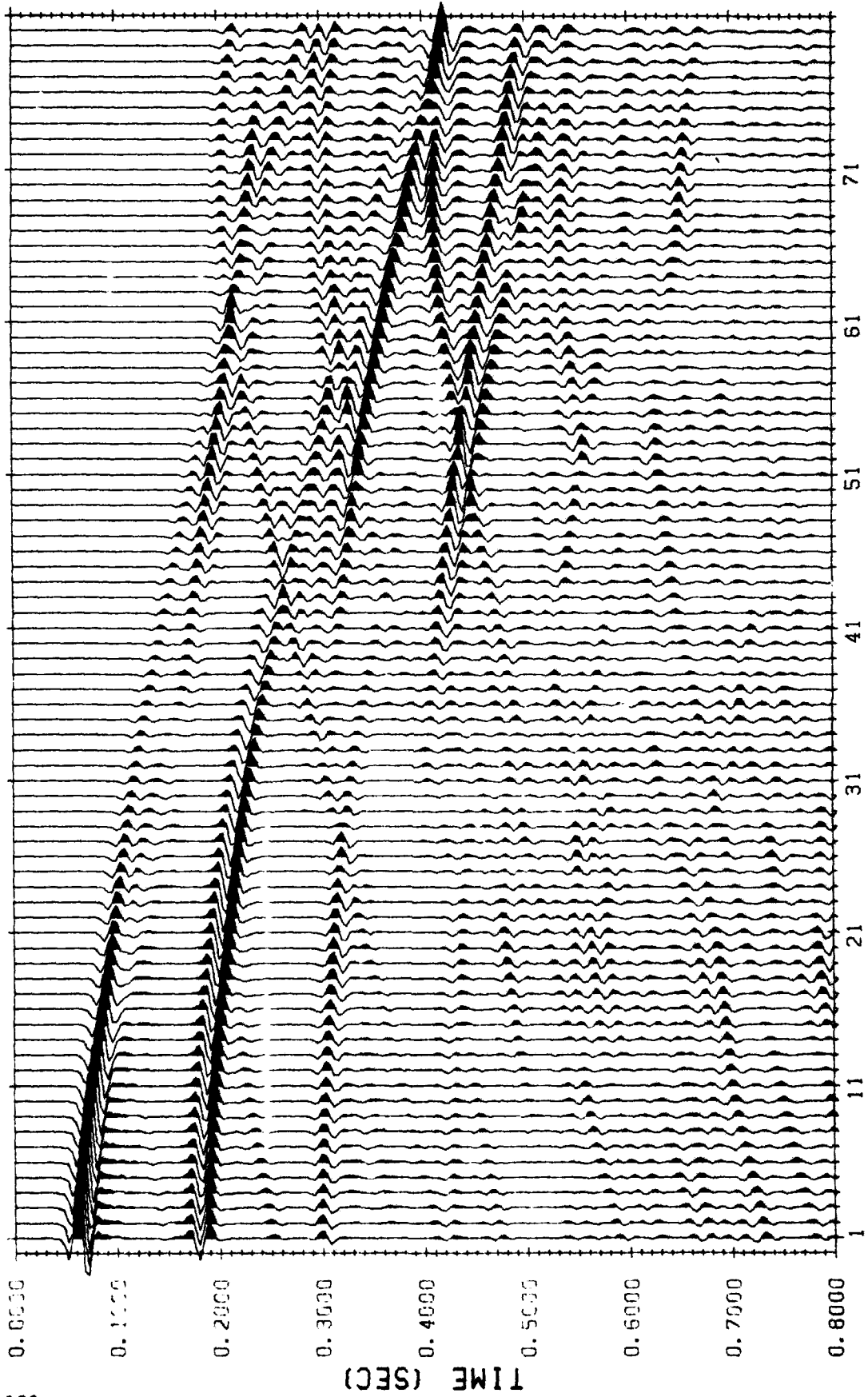


Figure 6
Model geometry for the basin model comparison between BINTEQ and QUIK shown in Figures 7 and 8.

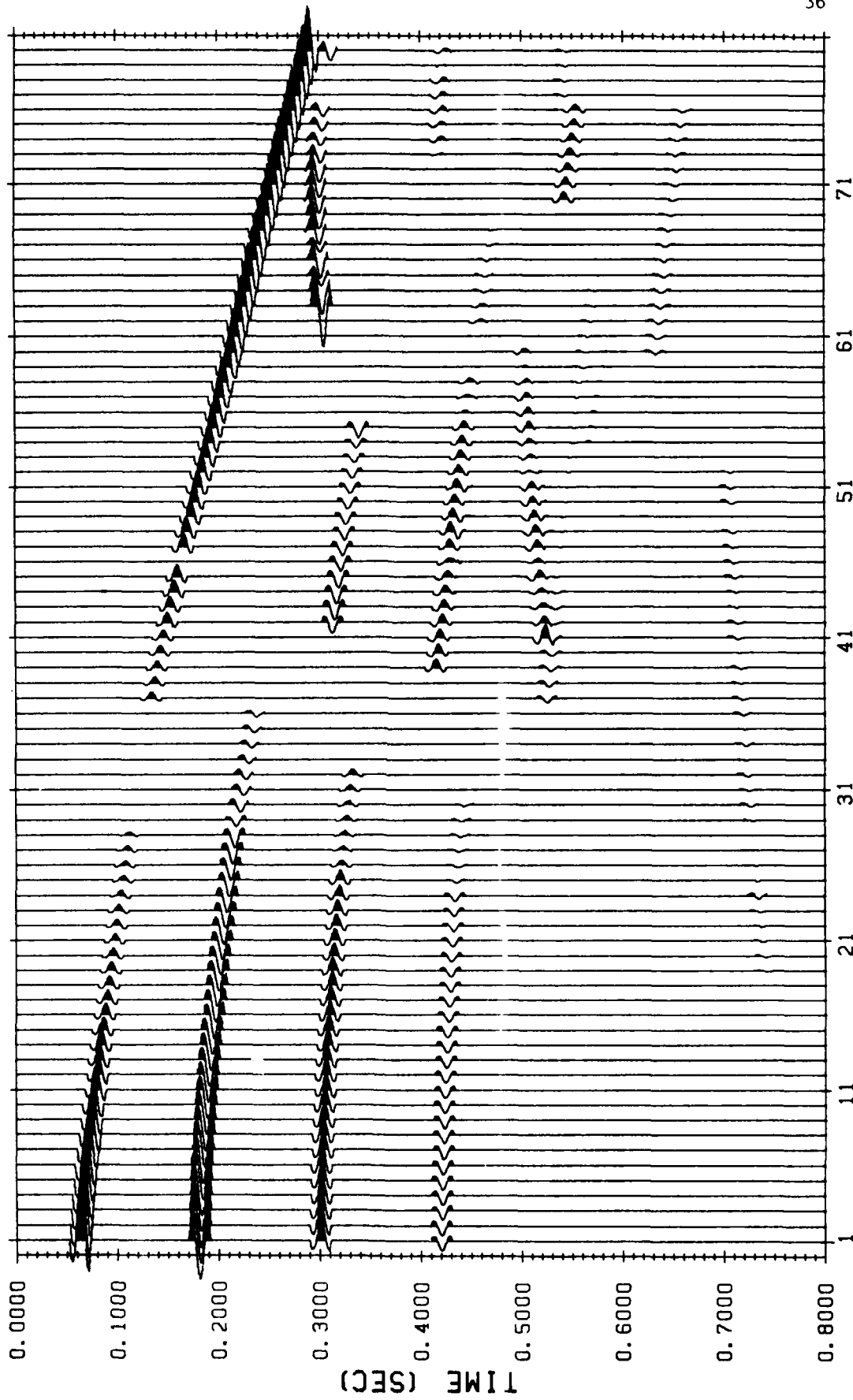
BINTEQ: SEISMIC SHOT RECORD FOR BASIN MODEL
COMPLETE SOLUTION FOR NEAR-SURFACE GROUPS
PRESSURE COMPONENT FOR POINT SOURCE AT 350 METER DEPTH



GROUP NUMBER

Figure 7
BINTEQ solution for the basin model shown in Figure 6.

QUIKSHOT: SEISMIC SHOT RECORD FOR BASIN MODEL
GEOMETRIC ARRIVALS FOR NEAR-SURFACE GROUPS
PRESSURE COMPONENT FOR POINT SOURCE AT 350 METER DEPTH



GROUP NUMBER

Figure 8
QUIK raytracing solution for the basin model shown in Figure 6.

left corner of the basin appears. The non-geometrical event that arrives early at the largest offsets in the BINTEQ solution is a head wave traveling at the faster velocity of 10 km/sec along the bottom of the basin. It is also interesting to note all the back scattered energy bouncing around in the basin.

The model for the last set of validation studies shown in this section is presented at the top of Figure 9. This more complex low-velocity wedge model was used by Koslov and Baysal (1982) to demonstrate the accuracy of the finite difference technique against a physical model. In the physical model, the low velocity wedge was submerged in water and pinched out against a plexiglass plate. The scaled seismic velocities used in the comparison are 4 km/sec in the top layer (water), 2.3 km/sec in the second layer (wedge) and 6 km/sec in the underlying layer (plate). The source is located under the free surface at a depth of 100 meters and an offset of 4440 meters. Receivers are located just under the free surface at a depth of 50 meters at offsets ranging between 750 to 5700 meters at an increment of 100 meters. The BINTEQ shot record is shown at the same scale as the model in Figure 9 and includes all arrivals in the frequency range of 4 to 30 Hz. The synthetic seismograms are shown as a function of time from 0.25 to 4.75 seconds so as to clip off the large impulse for the receivers near the source at zero time. The most important events are identified by numbers 1 through 17.

Event 1 is simply the direct arrival from the source plus the reflection off the free surface. Events 2 through 6 represent arrivals interacting with the wedge and the free surface: events 2, 4 and 6 are the primary reflection and the first and second multiple reflections off the wedge, respectively; event 3 represents the diffracted arrivals off corner B; and event 5 represents a twice diffracted arrival off corner B.

Events 7 through 12 represent arrivals involving primary reflections off the plate: event 7 is the primary off the plate transmitting through and diffracting off the wedge in the vicinity of corner C and traveling

resolve the sharp corner of the wedge with too few samples. The comparison was repeated with the 4th order finite difference algorithm of John Vidale at California Institute of Technology. The results from this comparison are shown in Figure 13 on the same scale as the BINTEQ and QUIK shot records in Figures 11 and 12. The agreement with this finite difference simulation is quite spectacular.

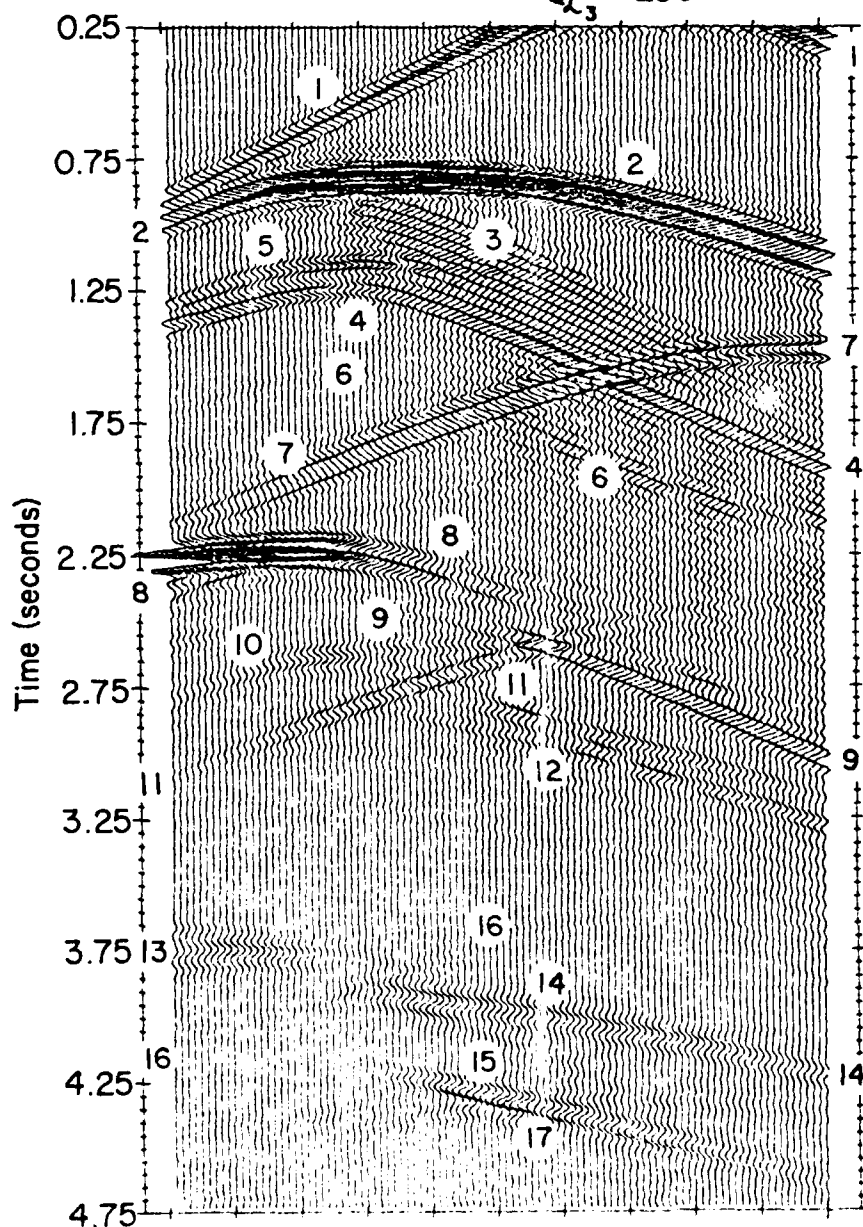
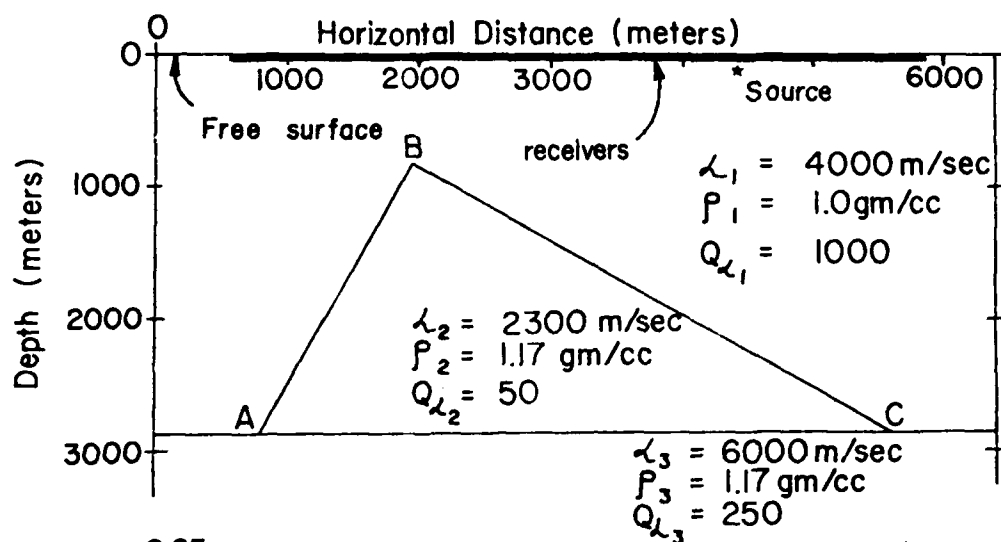


Figure 9
Model geometry for low-velocity wedge model comparison among BINTEG, QUIK, and two finite difference solutions shown in Figures 10 through 13.

**BINTEQ: SEISMIC SHOT RECORD FOR LOW-VELOCITY WEDGE MODEL
COMPLETE ACOUSTIC SOLUTION FOR NEAR-SURFACE GROUPS
PRESSURE COMPONENT FOR EXPLOSION DEPTH OF 100 METERS**

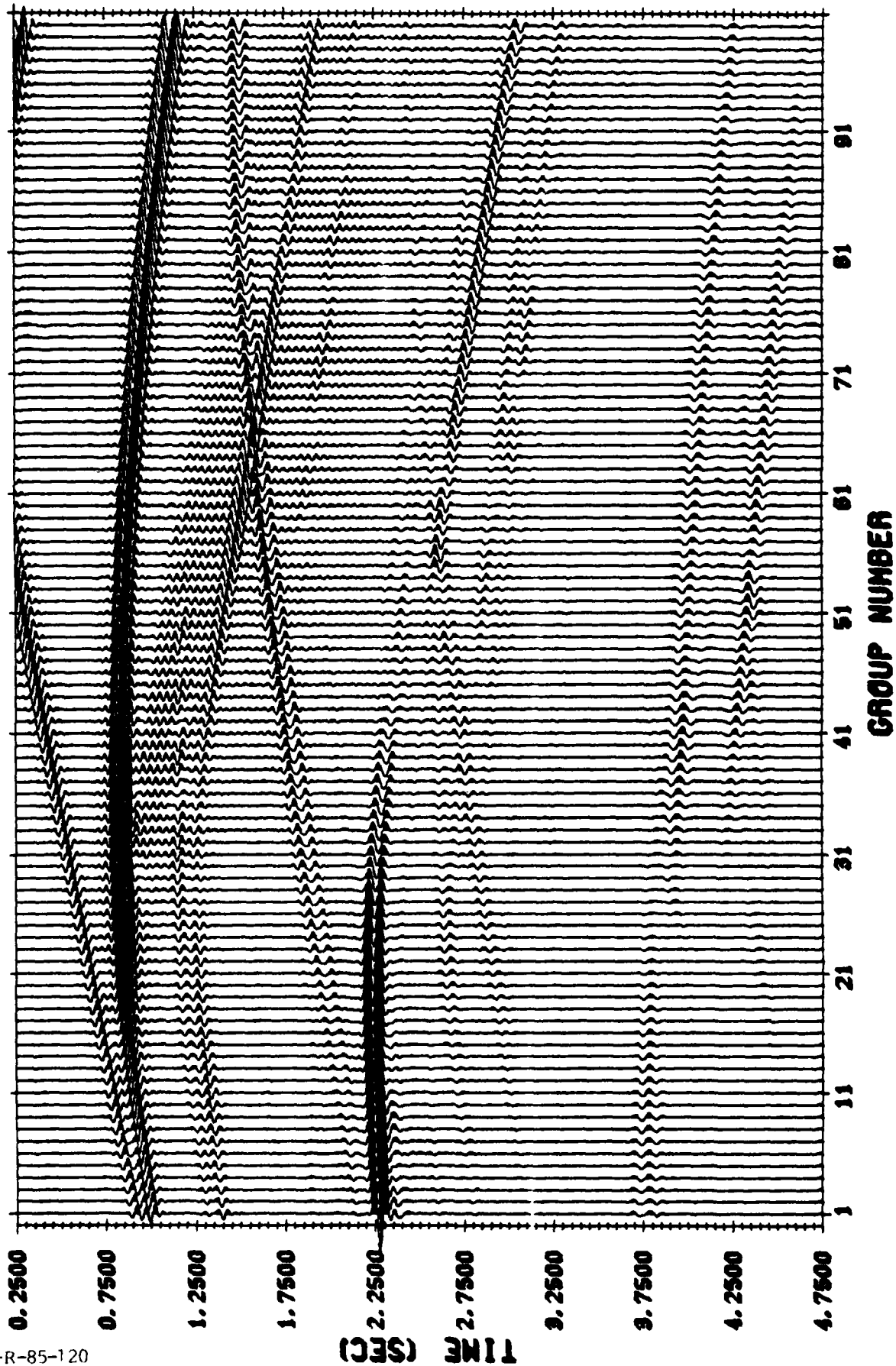


Figure 10
BINTEQ solution for the wedge model shown in Figure 9.

QUIKSHOT: SEISMIC SHOT RECORD FOR LOW-VELOCITY WEDGE MODEL
GEOMETRIC ARRIVALS FOR NEAR-SURFACE GROUPS
PRESSURE COMPONENT FOR POINT SOURCE AT 100 METER DEPTH

SGI-R-85-120

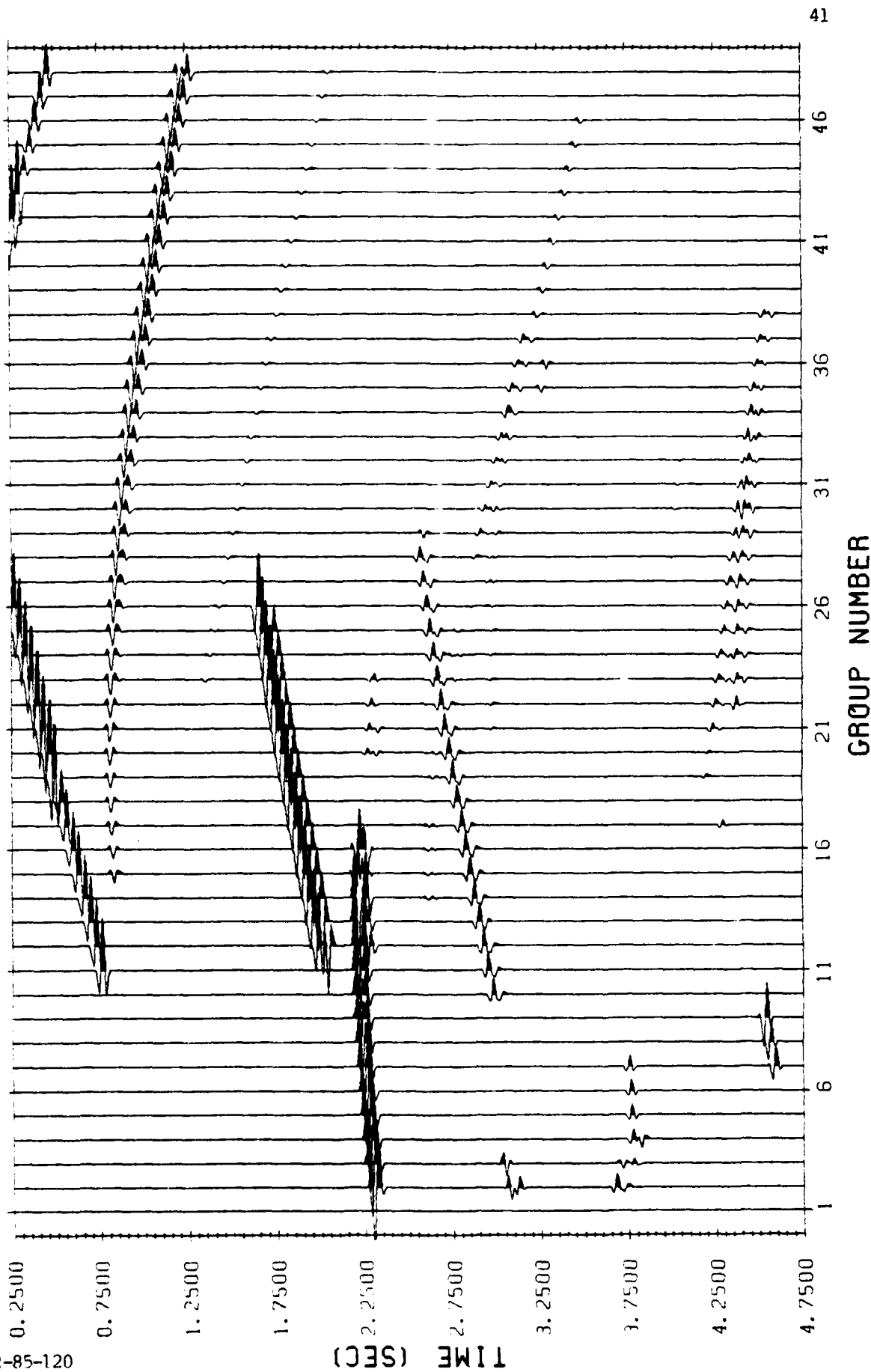


Figure 11
QUIK raytracing solution for the wedge model shown in Figure 9.

FOURIER FINITE-DIFFERENCE METHOD

SHOT RECORD FOR LOW-VELOCITY MODEL



GROUP NUMBER

Figure 12
Finite difference solution of Koslov and Baysal (1982) for the wedge model shown in Figure 9.

FINITE-DIFFERENCE METHOD SHOT RECORD FOR LOW-VELOCITY WEDGE MODEL



GROUP NUMBER

Figure 13
Finite difference solution of Vidale and Clayton (1984) for the wedge model shown in Figure 9.

3.2 CALCULATION FOR AFGL MODELS

The results from two sample calculations are presented in Figures 14 and 15 to show the effects of surface irregularities on the synthetic seismograms. Both 2-D models represent simple layer over half-space structures with a flat free surface and an irregular interface with compressional velocities of 4 and 8 km/sec, densities of 2.0 and 3.4 gm/cc and material quality factors of 50 and 1000 in the layer and the underlying half-space, respectively. The simulations have been carried out from 0 to 2.5 Hz and include all possible arrivals in the time window of 0 to 50 seconds. The models are shown to the left of the seismic sections with tick marks on the free surface denoting the location of receivers at model distances from 8 km to 94.4 km. The interfaces have been discretized at a sampling interval of 0.8 km for 128 points satisfying the minimum requirement of 2 sample points per wavelength at the highest frequency of interest. Both figures show true relative amplitudes except for a multiplicative scaling factor of the hypocentral distance to the power unity for display purposes only.

The results in Figure 14 can be used to examine the effects of irregularities on refracting horizons. A point isotropic source is located at a horizontal model distance of 10 km at a depth of 11 km, just one kilometer below the irregular interface. The results will be discussed with the aide of the labelled arrivals. First one can follow the direct arrival (A) as it moves out at the upper velocity of 4 km/sec. At about 20 km, arrival B emerges ahead of arrival A as it travels almost horizontally at the higher velocity of 8 km/sec before being refracted up to the free surface. As arrival B passes through the interface irregularities, it undergoes significant interference effects destroying the coherence of the phase and causing some back scattered energy (arrivals C). Then after passing through the irregularities, a coherent arrival re-emerges with a moveout of 8 km/sec (arrival D). The first multiple in the layer is arrival E and it is interesting to watch it merge with the direct arrival A at distances beyond about 70 km. Arrivals F and I represent back-scattered energy from the first multiple off the interface irregularities. At distances beyond about 72 km, the

BINTEQ2D-REV3.0: AFOSR MODEL MOD4-128

HORIZONTAL SEISMIC SECTION AT DEPTH (1) = 0.10000
 TYPE 2: X.Y (2) = 8.000 0.0000 TO X.Y (56) = 84.40 0.0000

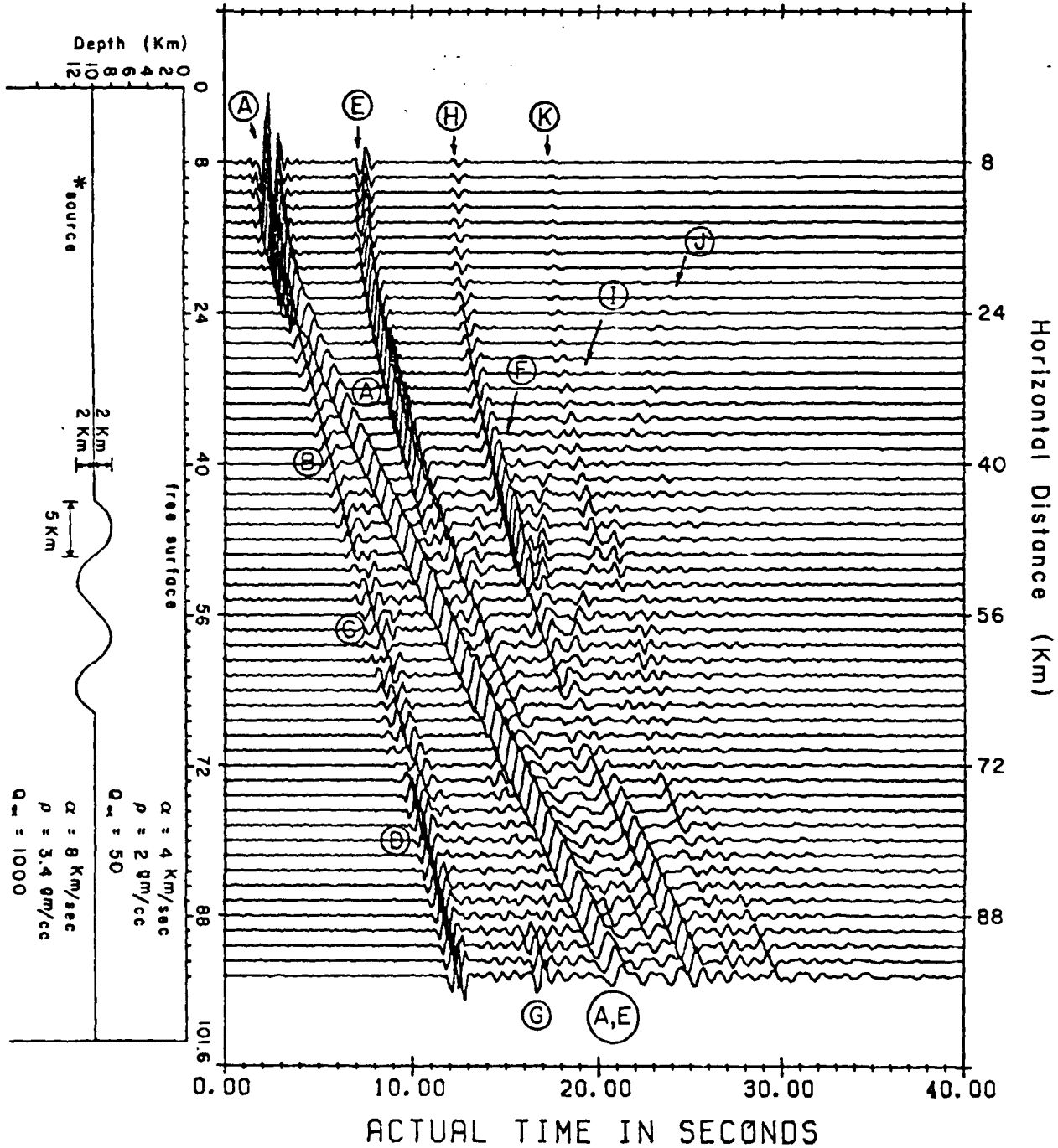


Figure 14. BINTEQ simulation (0-2.5 hz) of the seismic section for a point source located in the model shown at the left with surface irregularities on the second interface.

BINTEQ2D-REV3.0: AFOSR MODEL MOD3-128

HORIZONTAL SEISMIC SECTION AT DEPTH (1) = 0.10000
 TYPE 2: X,Y (1) = 8.000 0.0000 TO X,Y (55) = 84.40 0.0000

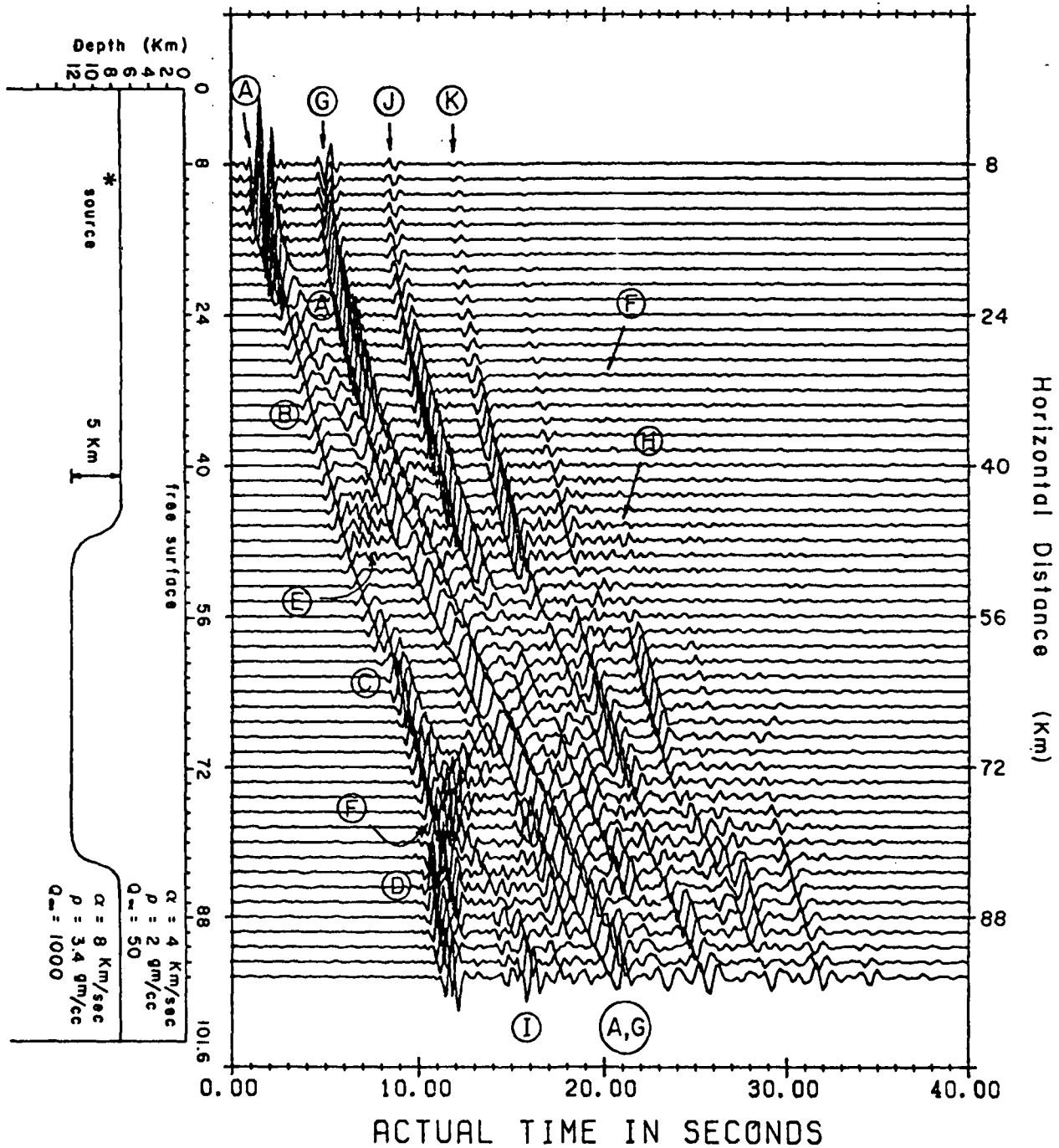


Figure 15. BINTeQ simulation (0-2.5 hz) of the seismic section for a point source located in the model shown at the left for a deep basin structure.

first multiple (arrival E) generates a head wave on the interface (arrival G) with a moveout of 8 km/sec. This arrival appears to grow beyond 90 km because of constructive interference from direct arrivals scattered toward the free surface at a moveout of 4 km/sec (arrivals originating between C and D). Arrivals H and K represent the next two higher order multiples in the layer and arrivals J plus other unmarked small arrivals represent more back scattered energy off the interface irregularities from these higher multiples.

The results in Figure 15 can be used to understand the effects of wave propagation through a basin. Direct arrivals A and B have the same interpretation as in Figure 14. In this figure, arrival C represents a true head wave off the bottom of the basin and arrival D represents a creeping wave corresponding to the continuation of arrival D past the eastern rise of the basin. The sequence of arrivals E represent diffractions off the rough corners of the discretely sampled western slope of the basin (and are not present at lower frequency where sampling is sufficient to emulate a smooth slope). As in the previous example, arrival F represents back-scattered energy off the eastern rise of the basin. Arrivals G, H and I are the first multiple, its back-scattered energy off eastern slope and its head wave generated after the eastern slope, analogous to arrivals E, F and G of the previous example. Arrivals J and K represent the next two higher order multiples and again the small back-scattered arrivals from these multiples are too small to demarcate.

In conclusion, BINTEQ has been verified through an exhaustive series of internal and external validation tests. Exact synthetic seismograms were shown for two models to study the influence of interface irregularities on seismic wave propagation in the earth. The most important findings from these studies are: 1) the interference effects observed from interface irregularities (arrivals C in Figure 2) may help explain the phase incoherence observed in real data from head wave energy along the Moho discontinuity; (2) significant back-scattered energy is to be expected from interface irregularities (arrivals F, I, J in Figure 14) and from basins (arrivals F, H in Figure 15); and (3) the

appearance and disappearance of critically refracted energy (arrivals G in Figure 14 and I in Figure 15) could easily have been misinterpreted in real data as a head wave from a deeper interface.

4.0 BINTEQ REFERENCES

- Apsel, R.J. (1979), Dynamic Green's functions for layered media and applications to boundary-value problems, Ph.D. Thesis, University of California at San Diego, 349 pp.
- Apsel, R.J. (1982), VESPA: Viscoelastic seismic profile algorithm for complete synthetic seismograms in layered media, Sierra Geophysics Technical Report, SGI-R-82-068, Contract N00014-81-C-0148
- Apsel, R.J., R.K. Wyss, G.R. Mellman and R.S. Hart (1983), Three-dimensional wave propagation using boundary integral equation techniques, Sierra Geophysics Technical Report, SGI-R-83-083 prepared for DARPA, 72 pp., Contract N00014-81-C-0148
- Berryhill, J.R. (1979), Wave equation datuming, Geophysics, 44, pp. 1329-1344.
- Cole, D.M. (1980), A numerical boundary integral equation method for transient motions, Ph.D. Thesis, Calif. Inst. of Tech., 228 pp.
- deHoop, A.T., 1958, Representation theorems for displacement in an elastic solid and their application to elastodynamic diffraction theory, D.Sc. Thesis, Technische Hogeschool, Delft, The Netherlands.
- Ferguson, J.F. (1981), Geophysical investigations of Yucca Flat, Nevada, Ph.D. Thesis, Southern Methodist University.
- Lundquist, G.M., S.K. Kaufman and G.R. Mellman (1982), Three-dimensional raytracing, Abstract in Technical Program of Society of Exploration Geophysics 52nd Annual International Meeting, Dallas, Texas, pp. 212-213.

- Koslov, D.D. and E. Baysal (1982), Forward modeling by a Fourier method, Geophysics, 47, pp. 1402-1412.
- Mellman, G.R., R.S. Hart, G.M. Lundquist and D.M. Hadley (1982), Investigations of near-source structural effects on body waves, Part I-Yucca Flats, Sierra Geophysics Technical Report, SGI-R-82-058 prepared for DARPA, 59 pp., Contract F08606-79-C-0009.
- Morse, P.M. and H. Feshbach (1953), Methods of Theoretical Physics, McGraw Hill Book Company, Inc., 1978 pp.
- Schuster, G.T. (1984), Some boundary integral equation methods and their application to seismic exploration, Draft of Ph.D. Thesis, Columbia University, 132 pp.
- Scott, P. and D.V. Helmberger (1983), Applications of the Kirchhoff-Helmholtz integral to problems in seismology, Geophys. J.R. astr. Soc., 72, pp. 237-254.

END

FILMED

3-86

DTIC